

Stochastic Thermodynamics at the Quantum-Classical Boundary: A Self-Consistent Framework Based on Adiabatic-Response Theory

Joshua Eglinton^{1,2}, Federico Carollo³, Igor Lesanovsky^{1,2,3} and Kay Brandner^{1,2*}

¹*School of Physics and Astronomy, University of Nottingham, Nottingham NG7 2RD, United Kingdom*

²*Centre for the Mathematics and Theoretical Physics of Quantum Non-equilibrium Systems,
University of Nottingham, Nottingham NG7 2RD, United Kingdom*

³*Institut für Theoretische Physik, Eberhard Karls Universität Tübingen,
Auf der Morgenstelle 14, 72076 Tübingen, Germany*

(Dated: April 17, 2024)

Microscopic thermal machines promise to play an important role in future quantum technologies. Making such devices widely applicable will require effective strategies to channel their output into easily accessible storage systems like classical degrees of freedom. Here, we develop a self-consistent theoretical framework that makes it possible to model such quantum-classical hybrid devices in a thermodynamically consistent manner. Our approach is based on the assumption that the quantum part of the device is subject to strong decoherence and dissipation induced by a thermal reservoir. Due to the ensuing separation of time scales between slowly evolving classical and fast relaxing quantum degrees of freedom, the dynamics of the hybrid system can be described by means of adiabatic-response theory. We show that, upon including fluctuations in a minimally consistent way, the resulting equations of motion can be equipped with a first and second law, both on the ensemble level and on the level of individual trajectories of the classical part of the system, where thermodynamic quantities like heat and work become stochastic variables. As an application of our theory, we work out a physically transparent model of a quantum-classical hybrid engine, whose working system consists of a chain of Rydberg atoms, which is confined in an optical cavity and driven by periodic temperature variations. We show by means of numerical simulations that the engine can sustain periodic oscillations of a movable mirror, which acts as a classical load, against external friction and extract the full distributions of input heat and output work. By making the statistics of thermodynamic processes in quantum-classical hybrid systems accessible without the need to further specify a measurement protocol, our work contributes towards bridging the long-standing gap between classical and quantum stochastic thermodynamics.

I. INTRODUCTION

Thermal machines have played a central role in the development of classical thermodynamics, whose early pioneers sought to uncover the fundamental principles that determine the performance of devices like heat engines or refrigerators. Almost two centuries later, understanding the working mechanisms of microscopic thermal machines, which operate on atomistic length and energy scales, and unlocking their potential for future applications have become major driving forces of quantum thermodynamics [1–5]. The last decade has seen remarkable progress in this direction. On the theory side, a whole spectrum of new concepts has emerged, for example to exploit collective effects in quantum many-body systems for power generation and cooling [6–30], to identify optimal control strategies for quantum thermodynamic cycles [30–45], to reduce fluctuations in quantum thermal machines [24, 46–53], or to channel their output into externally accessible storage systems [54–61]. On the experimental side, microscopic thermal machines have been realized on a whole variety of different platforms including single atoms and ions [61–63], ultracold atomic gases [64, 65], semiconductor nano-structures [66], supercon-

ducting devices [67], photonic systems [68] and nuclear spins [69, 70].

These developments have transformed our conceptual understanding of both the very nature of thermal machines and the criteria by which their performance should be assessed. Besides traditional figures of merit such as power and efficiency, the list of desirable properties now includes scalability, i.e., the ability to increase outputs by enlarging working systems, constancy, i.e., resilience against thermal and quantum fluctuations, and exploitability, i.e., the possibility to access and store generated outputs. Addressing as many as possible of these criteria at the same time is a challenging endeavour, which quickly leads to fundamental problems. Quantities like work and heat, for example, can in general not be measured in quantum systems without altering their state or even their internal energy [71–78]. As a result, the actual output of quantum thermal machines can, even in theory, only be determined in the context of specific measurement protocols, which can be hard to implement in practice and do not necessarily reflect realistic working conditions [71–79].

An elegant means of circumventing this problem would be to channel the output of quantum thermal machines into classical systems, which, at least in principle, can be monitored without perturbing their state. However, this idea immediately leads to the question of how to describe the dynamics of hybrid systems with both classi-

* kay.brandner@nottingham.ac.uk

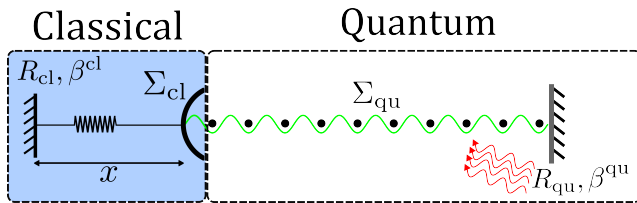


FIG. 1. Quantum-classical hybrid system. The classical and the quantum subsystem, Σ_{cl} and Σ_{qu} , respectively consist of a movable mirror and a chain of Rydberg atoms inside an optical cavity. Both subsystems are coupled to thermal reservoirs, R_{cl} and R_{qu} , with inverse temperatures β^{cl} and β^{qu} .

cal and quantum degrees of freedom, which, despite longstanding efforts has not been fully settled so far [80–100]. Here, we seek to address this problem from the perspective of quantum thermodynamics. Our approach is based on the assumption that the quantum degrees of freedom are coupled to a thermal reservoir, which induces strong damping and decoherence on a fast time scale. As a result, the state of the quantum subsystem remains close to thermal equilibrium, even under the influence of classical degrees of freedom, which can typically be assumed to evolve on much slower time scales than the quantum ones. At the same time, any measurement-induced back-action from the classical on the quantum subsystem becomes negligible compared to reservoir-induced decoherence. Under these conditions, the evolution of the quantum degrees of freedom can be described by means of adiabatic perturbation theory, a general method to describe systems with well separated time scales, which has been used before to model quantum-classical hybrid dynamics [100–102] and has recently been deployed very successfully in quantum thermodynamics [30, 32–37, 50, 102–104]. The effective force that is exerted by the quantum subsystem on the classical one, which can in principle be driven arbitrarily far from equilibrium, can then be inferred from energy conservation. Upon including fluctuations in a minimal thermodynamically consistent way, it thus becomes possible to construct a self-consistent framework that describes the dynamics and thermodynamics of quantum-classical hybrid systems in terms of stochastic equations of motion and a first and a second law. Furthermore, since the classical degrees of freedom follow well-defined observable trajectories, a concept that does in general not exist for quantum systems, these laws can be formulated on the level of ensembles and for individual realizations of the dynamics. Thermodynamic processes can therefore be analyzed in a statistical manner, where quantities like work and heat become stochastic variables, whose full distributions can, at least in principle, be inferred by observing only the classical degrees of freedom. As a result, many of the established concepts of classical stochastic thermodynamics [105–107] can be directly applied to quantum-classical hybrid systems. In the context of thermal machines, for instance, output fluctuations can be determined by observing the trajec-

tories of a classical load. Constancy, as a third figure of merit besides power and efficiency [46], thus becomes a directly accessible parameter without the need of further specifying a measurement protocol.

From a practical perspective, it is important to identify suitable experimental platforms, on which quantum-classical hybrid machines can be implemented and theoretical predictions can be tested. Although such experiments can generally be expected to be challenging, optomechanical systems, which can be realized in a variety of different ways [108], for example, with cold atoms [109–111], photonic crystals [112], or superconductors coupled to micro-mechanical membranes [113], provide a natural starting point. In the second part of this article, we therefore analyze a physically transparent model of a quantum-classical hybrid engine, whose classical degree of freedom consists of a movable mirror, which, together with a second fixed mirror, forms an optical cavity. The quantum part of the engine is formed by a long chain of Rydberg atoms, whose large internal energy scale makes them natural candidates for quantum systems that can plausibly exert an observable effect on a classical object [114]. Similar to a recent experiment, where a quantum heat engine was realized on the platform of super-radiant atoms [6], the interaction between the two subsystems is mediated by the radiation pressure inside the cavity. Upon being provided with input from a noisy laser, which mimics a thermal reservoir, the machine can sustain periodic oscillations of the movable mirror, which plays the role of a classical load, against classical friction, see Fig. 1. As we show by means of numerical simulations, our framework makes it possible to obtain the full distributions of output work and effective input heat for this model, which illustrates the potential of our theory to open a new perspective on the stochastic thermodynamics of quantum systems.

II. DYNAMICAL FRAMEWORK

We first consider a generic hybrid system that consists of a quantum subsystem Σ_{qu} and a classical subsystem Σ_{cl} in contact with their respective reservoirs R_{qu} and R_{cl} whose inverse temperatures are β^{qu} and β^{cl} , see Fig. 1. The two subsystems are mechanically coupled so that the Hamiltonian of Σ_{qu} depends on the state of Σ_{cl} . In this section we develop a general framework to describe the non-equilibrium dynamics of this setup. Our approach is based on the assumption that the characteristic timescales of the classical and quantum subsystems, that is the observational timescales, $\tau^{\Sigma_{cl}}$ and $\tau^{\Sigma_{qu}}$, on which the state of Σ_{cl} and Σ_{qu} change significantly, are well separated. As we will show in the next section, the resulting dynamical framework is fully consistent with the laws of thermodynamics.

1. Quantum dynamics

We initially consider the state of the classical subsystem Σ_{cl} to be frozen. The quantum subsystem can then be regarded as an open system, whose Hamiltonian H_x^{qu} depends on a fixed external parameter x , for instance the position of a movable mirror of an optical cavity. We take the Hilbert space of the quantum subsystem to be finite-dimensional throughout. The state of Σ_{qu} is described by the density matrix ρ , which evolves in time according to the quantum master equation

$$\dot{\rho}_t = \mathcal{L}_x \rho_t. \quad (1)$$

In the weak-coupling limit, on which we focus here, the generator \mathcal{L}_x has the generic form

$$\mathcal{L}_x \circ = \mathcal{H}_x \circ + \mathcal{D}_x \circ \quad (2)$$

with the two superoperators

$$\mathcal{H}_x \circ = -\frac{i}{\hbar} [H_x^{\text{qu}}, \circ] - \frac{i}{\hbar} [H_x^{\text{LS}}, \circ], \quad (3a)$$

$$\mathcal{D}_x \circ = \sum_j \left\{ \gamma_x^{j-} \mathcal{K}[L_x^j] \circ + \gamma_x^{j+} \mathcal{K}[L_x^{j\dagger}] \circ \right\}, \quad (3b)$$

where we have introduced the short-hand notation

$$\mathcal{K}[Y] \circ = Y \circ Y^\dagger - Y^\dagger Y \circ / 2 - \circ Y^\dagger Y / 2. \quad (4)$$

The Lamb shift H_x^{LS} and the Lindblad operators L_x and L_x^\dagger account for the influence of the reservoir R_{qu} on Σ_{qu} and have the following properties. The Lamb shift commutes with the Hamiltonian of the quantum subsystem H_x^{qu} and therefore only induces corrections to its Bohr frequencies. The Lindblad operators induce jumps between energy levels of H_x^{qu} , during which the system absorbs or emits the energy $\hbar\nu_x^j \geq 0$. That is, we have

$$[H_x^{\text{qu}}, H_x^{\text{LS}}] = 0, \quad (5a)$$

$$[H_x^{\text{qu}}, L_x^j] = -\hbar\nu_x^j L_x^j, \quad [H_x^{\text{qu}}, L_x^{j\dagger}] = \hbar\nu_x^j L_x^{j\dagger}. \quad (5b)$$

Micro-reversibility further requires the dissipation rates γ_x^{j+} and γ_x^{j-} to obey the detailed balance condition

$$\gamma_x^{j+} / \gamma_x^{j-} = \exp[-\beta^{\text{qu}} \hbar\nu_x^j], \quad (6)$$

which is required for thermodynamic consistency. We note that the conditions (5) and (6) require that the Lamb shift, the Lindblad operators and the dissipation rates are dependent on x , since H_x^{qu} depends on x . As long as this parameter is fixed, the stationary solution of the master equation (2) is given by the Gibbs state

$$\varrho_x^{\text{qu}} \equiv \exp\left[-\beta^{\text{qu}}(H_x^{\text{qu}} - \mathcal{F}_x)\right], \quad (7)$$

where \mathcal{F}_x is the free energy of the quantum subsystem.

2. Classical subsystem

We now identify the parameter x with the position of the classical subsystem Σ_{cl} , whose full state is described by the phase space vector $\mathbf{z} \equiv (x, p)$ and whose time evolution is governed by the Langevin equations

$$\dot{x}_t = p_t / m, \quad (8a)$$

$$\dot{p}_t = -U'_{x_t} + f_{\mathbf{z}_t}^{\text{qu}} - \zeta^{\text{cl}} p_t + \xi_t^{\text{cl}}. \quad (8b)$$

Here, m denotes the mass of the classical degree of freedom, U_x is an external potential and primes denote derivatives with respect to x . Furthermore, $f_{\mathbf{z}}^{\text{qu}}$ denotes the force that the quantum subsystem exerts on the classical one. The Gaussian stochastic force ξ_t^{cl} , which together with the friction constant ζ^{cl} accounts for the influence of the classical reservoir R_{cl} , obeys

$$\langle \xi_t^{\text{cl}} \rangle = 0 \quad \text{and} \quad \langle \xi_t^{\text{cl}} \xi_{t'}^{\text{cl}} \rangle \equiv 2D^{\text{cl}} \delta_{t-t'}, \quad (9)$$

where δ_t denotes Dirac delta. The diffusion constant D^{cl} is thereby related to the friction constant ζ^{cl} through the fluctuation-dissipation theorem [115]

$$D^{\text{cl}} = \zeta^{\text{cl}} m / \beta^{\text{cl}}. \quad (10)$$

3. Quantum coupling force

To determine the coupling force $f_{\mathbf{z}}^{\text{qu}}$, we assume that x_t varies slowly on the relaxation timescale of the quantum subsystem Σ_{qu} . Under this condition, the time evolution of Σ_{qu} can be described in terms of an adiabatic quantum master equation [103], which can be obtained from Eq. (1) by replacing $x \rightarrow x_t$. The solution of this equation can be found by means of adiabatic perturbation theory. Here we use the second-order ansatz

$$\rho_t = \varrho_{x_t}^{\text{qu}} + \rho_{x_t}^{(x)} p_t + \rho_{x_t}^{(2x)} p_t^2 + \rho_{x_t}^{(p)} \dot{p}_t \quad (11)$$

for the state of Σ_{qu} [35, 103, 104], which will turn out to be a minimal consistent choice. Insertion into the adiabatic master equation yields

$$\rho_x^{(x)} = \frac{1}{m} \mathcal{L}_x^{-1} \varrho_x^{\text{qu}'}, \quad \rho_x^{(2x)} = \frac{1}{m} \mathcal{L}_x^{-1} \rho_x^{(x)'}, \quad \rho_x^{(p)} = \mathcal{L}_x^{-1} \rho_x^{(x)}, \quad (12)$$

where we assume that ϱ_x^{qu} is the only stationary state of the frozen generator \mathcal{L}_x such that the super-operator inverse in Eqs. (12) is well defined [116]. This approach is justified if x changes slowly on the relaxation timescale $\tau^{\Sigma_{\text{qu}}}$ of the quantum subsystem. That is, we assume the timescale $\tau^{\Sigma_{\text{cl}}}$ is large compared with the quantum relaxation timescale set by the rates γ_x^{j+} and γ_x^{j-} .

The systematic part of the coupling force $f_{\mathbf{z}}^{\text{qu}}$ reads

$$\langle f_{\mathbf{z}}^{\text{qu}} \rangle = \text{Tr}[F_x \rho] \quad \text{with} \quad F_x \equiv -H_x^{\text{qu}'} \quad (13)$$

playing the role of a quantum force operator. This expression must be evaluated using the first-order adiabatic

expansion of ρ_t , so that it can be consistently interpreted as a force acting on the classical degree of freedom, which depends only on its position and velocity, but not on acceleration.

We thus obtain

$$\langle f_{\mathbf{z}}^{\text{qu}} \rangle = \text{Tr}[F_x \varrho_x^{\text{qu}}] + \text{Tr}[F_x \rho_x^{(x)}] p = -\mathcal{F}'_x - \zeta_x^{\text{qu}} p, \quad (14)$$

with the quantum friction constant

$$\zeta_x^{\text{qu}} = -\text{Tr}[F_x \rho_x^{(x)}]. \quad (15)$$

The quantum friction force has to be counterbalanced by the fluctuating force $\xi_{x,t}^{\text{qu}} = f_{\mathbf{z},t}^{\text{qu}} - \langle f_{\mathbf{z},t}^{\text{qu}} \rangle$ which we assume to be Gaussian and uncorrelated with the classical fluctuating force. Hence, we set

$$\langle \xi_{x,t}^{\text{qu}} \rangle = \langle \xi_{x,t}^{\text{qu}} \xi_{x,t'}^{\text{cl}} \rangle = 0 \quad \text{and} \quad \langle \xi_{x,t}^{\text{qu}} \xi_{x,t'}^{\text{qu}} \rangle = 2D_x^{\text{qu}} \delta_{t-t'}. \quad (16)$$

The quantum diffusion constant D_x^{qu} can now be identified with the equilibrium correlation function

$$\begin{aligned} D_x^{\text{qu}} &= \int_0^\infty dt \langle \langle \delta \hat{F}_{x,t}; \delta \hat{F}_{x,0} \rangle \rangle_{\varrho^{\text{qu}}} \\ &= -\langle \langle (\mathbf{L}_x^\dagger)^{-1} \delta F_x; \delta F_x \rangle \rangle_{\varrho^{\text{qu}}} \geq 0, \end{aligned} \quad (17)$$

where $\delta F_x = F_x + \mathcal{F}'_x$ and hats indicate Heisenberg-picture operators [102]. The super-operator \mathbf{L}_x^\dagger is the adjoint of \mathbf{L}_x with respect to the Hilbert-Schmidt scalar product and the Kubo correlation function that appears in Eq. (17) is defined as [115]

$$\langle \langle \circ; \bullet \rangle \rangle_Y \equiv \int_0^1 d\lambda \text{Tr}[\circ^\dagger Y^\lambda \bullet Y^{1-\lambda}]. \quad (18)$$

We note that, in contrast to a symmetrized correlation function, which would have been a second natural choice for D_x^{qu} , the Kubo correlation function ensures that the fluctuation-dissipation theorem

$$D_x^{\text{qu}} = \zeta_x^{\text{qu}} m / \beta^{\text{qu}} \quad (19)$$

holds. As we will see in the following, this condition is necessary for the system to relax to a global thermal equilibrium state, which is free of dissipative currents, if $\beta^{\text{qu}} = \beta^{\text{cl}}$. The total coupling force between the classical and quantum subsystem is now given by

$$f_{\mathbf{z},t}^{\text{qu}} = -\mathcal{F}'_x - \zeta_x^{\text{qu}} p + \xi_{x,t}^{\text{qu}}, \quad (20)$$

where the fluctuating force $\xi_{x,t}^{\text{qu}}$ is fully characterized by the relations (16) and (19). We therefore have a complete dynamical model of our quantum-classical hybrid system.

4. Fokker-Planck equation

The classical probability density $P_{\mathbf{z},t}$ of finding Σ_{cl} in the state $\mathbf{z} = (x, p)$ obeys the Fokker-Planck equation

$$\dot{P}_{\mathbf{z},t} = -\partial_x j_{\mathbf{z},t}^x - \partial_p j_{\mathbf{z},t}^p, \quad (21)$$

where the probability currents $j_{\mathbf{z},t}^x \equiv j_t^x$ and $j_{\mathbf{z},t}^p \equiv j_t^p$ are defined as

$$j_t^x \equiv \frac{p}{m} P_t \quad (22a)$$

$$j_t^p \equiv \left(U'_x + \mathcal{F}'_x + (\zeta^{\text{cl}} + \zeta_x^{\text{qu}}) p + (D^{\text{cl}} + D_x^{\text{qu}}) \partial_p \right) P_t \quad (22b)$$

with $P_t \equiv P_{\mathbf{z},t}$. Once the solution of Eq. (21) for a given initial distribution has been found, the average of an arbitrary observable $A_{\mathbf{z}}$ of the system can be evaluated as

$$\langle A_{\mathbf{z}} \rangle_t = \int d\mathbf{z} \text{Tr}[A_{\mathbf{z}} \rho_{\mathbf{z},t}]. \quad (23)$$

The extended density matrix $\rho_{\mathbf{z},t}$, which describes the joint state of Σ_{qu} and Σ_{cl} , thereby depends explicitly on the phase-space variables \mathbf{z} and is given by

$$\rho_{\mathbf{z},t} \equiv \varrho_x^{\text{qu}} P_t + \rho_x^{(x)} p P_t + \rho_x^{(2x)} p^2 P_t + \rho_x^{(p)} j_t^p. \quad (24)$$

This expression follows by interpreting the density matrix given in Eq. (11) as describing the state of the quantum subsystem under the condition that the values of the classical phase space variables x_t , p_t and \dot{p}_t are known. Since the adiabatic-response corrections defined in Eq. (12) are all traceless, $\rho_{\mathbf{z},t}$ satisfies the normalization conditions

$$\text{Tr}[\rho_{\mathbf{z},t}] = P_t \quad \text{and} \quad \int d\mathbf{z} \text{Tr}[\rho_{\mathbf{z},t}] = 1. \quad (25)$$

In equilibrium, i.e., for $\beta^{\text{qu}} = \beta^{\text{cl}} = \beta$, the stationary solution of Eq. (21) is

$$P_{\text{eq}} = \exp \left[-\beta (H_{\mathbf{z}}^{\text{cl}} + \mathcal{F}_x - \mathcal{F}_{\mathbf{z}}^{\text{cl}}) \right] \quad (26)$$

with the Hamiltonian of the classical subsystem

$$H_{\mathbf{z}}^{\text{cl}} \equiv U_x + p^2/2m \quad (27)$$

and the classical free energy $\mathcal{F}_{\mathbf{z}}^{\text{cl}}$. The equilibrium state of the quantum-classical system is thus described by the extended density matrix

$$\begin{aligned} \rho_{\text{eq}} &= \exp \left[-\beta (H_x^{\text{qu}} + H_{\mathbf{z}}^{\text{cl}} - \mathcal{F}_{\mathbf{z}}^{\text{cl}}) \right] \\ &\quad + \left(\rho_x^{(x)} p + \rho_x^{(2x)} p^2 - \rho_x^{(p)} (U'_x + \mathcal{F}'_x) \right) P_{\text{eq}}, \end{aligned} \quad (28)$$

where the first line corresponds to $\varrho_x^{\text{qu}} P_{\text{eq}}$ and the corrections in the second line account for the finite relaxation time of Σ_{qu} .

III. THERMODYNAMIC FRAMEWORK

We now show how the dynamical framework developed in the previous section can be furnished with a consistent thermodynamic structure, first on the ensemble level, and then on the level of individual trajectories of the classical subsystem. In the second part, we focus on applications of our theory to hybrid thermal machines.

A. Ensemble thermodynamics

1. First law

Since the quantum-classical system is autonomous, the first law takes the form

$$\dot{E}_t = \dot{Q}_t^{\text{qu}} + \dot{Q}_t^{\text{cl}}, \quad (29)$$

where E_t denotes the internal energy of the total system and $\dot{Q}_t^{\text{qu/cl}}$ corresponds to the rate of heat uptake from the reservoir $R_{\text{qu/cl}}$. To derive explicit expressions for these quantities, we identify the internal energy of the quantum-classical system as

$$E_t = \langle H_x^{\text{qu}} + H_{\mathbf{z}}^{\text{cl}} \rangle_t. \quad (30)$$

The total rate of heat uptake then becomes

$$\begin{aligned} \dot{E}_t &= \int d\mathbf{z} \left\{ \text{Tr}[H_x^{\text{qu}} \dot{\rho}_{\mathbf{z},t}] + H_{\mathbf{z}}^{\text{cl}} \dot{P}_t \right\} \\ &\simeq \int d\mathbf{z} \left\{ \text{Tr}[H_x^{\text{qu}} \psi_{\mathbf{z}}] + H_{\mathbf{z}}^{\text{cl}} \right\} \dot{P}_t, \end{aligned} \quad (31)$$

where we have introduced the abbreviation

$$\psi_{\mathbf{z}} \equiv \varrho_x^{\text{qu}} + \rho_x^{(x)} p \quad (32)$$

and the time derivative of the extended density matrix has been taken in first order in the adiabatic expansion (24) so that \dot{E}_t is consistently obtained to second order. Upon inserting the Fokker-Planck equation (21) into (31) and integrating by parts with respect to x and p , we find

$$\begin{aligned} \dot{E}_t &= \int d\mathbf{z} \left\{ \text{Tr}[H_x^{\text{qu}} \mathbb{L}_x \rho_{\mathbf{z},t}] + (\zeta_x^{\text{qu}} p + U'_x + \mathcal{F}'_x) j_t^x + \frac{p}{m} j_t^p \right\} \\ &= \int d\mathbf{z} \left\{ \text{Tr}[H_x^{\text{qu}} \mathbb{L}_x \rho_{\mathbf{z},t}] - \frac{\zeta^{\text{cl}} p^2 + D^{\text{cl}} + D_x^{\text{qu}}}{m} P_t \right\}, \end{aligned} \quad (33)$$

where we have used the relation

$$j_t^x \partial_x \psi_{\mathbf{z}} + j_t^p \partial_p \psi_{\mathbf{z}} = \mathbb{L}_x \rho_{\mathbf{z},t}. \quad (34)$$

The final expression in Eq. (33) follows by inserting Eq. (22a) and integrating by parts with respect to p . This result leads us to identify \dot{Q}_t^{qu} and \dot{Q}_t^{cl} as

$$\dot{Q}_t^{\text{qu}} = \int d\mathbf{z} \left\{ \text{Tr}[H_x^{\text{qu}} \mathbb{L}_x \rho_{\mathbf{z},t}] + \frac{D_x^{\text{qu}}}{m} P_t \right\}, \quad (35a)$$

$$\dot{Q}_t^{\text{cl}} = \int d\mathbf{z} \left\{ D^{\text{cl}} - \zeta^{\text{cl}} p^2 \right\} \frac{P_t}{m}. \quad (35b)$$

It is straightforward to check, by substituting Eq. (28) into these identifications, that both the quantum and classical heat currents vanish in equilibrium, i.e., for $\beta^{\text{qu}} = \beta^{\text{cl}}$.

2. Second law

To show that the expressions (35) for the heat currents are consistent with the second law, we identify the entropy of the hybrid system as [117]

$$S_t = - \int d\mathbf{z} \text{Tr}[\rho_{\mathbf{z},t} \ln \rho_{\mathbf{z},t}]. \quad (36)$$

The rate of entropy production in the system then becomes

$$\begin{aligned} \dot{S}_t &= - \int d\mathbf{z} \text{Tr}[\dot{\rho}_{\mathbf{z},t} \ln \rho_{\mathbf{z},t}] \\ &\simeq - \int d\mathbf{z} \text{Tr}[\psi_{\mathbf{z}} \ln \rho_{\mathbf{z},t}] \dot{P}_t \\ &= - \int d\mathbf{z} \text{Tr}[(\mathbb{L}_x \rho_{\mathbf{z},t}) \ln \rho_{\mathbf{z},t} + \psi_{\mathbf{z}} (j_t^x \partial_x + j_t^p \partial_p) \ln \rho_{\mathbf{z},t}], \end{aligned} \quad (37)$$

(38)

where we have again used the Fokker-Planck equation (21), integrated by parts with respect to phase-space variables and inserted the identity (34). Upon expanding to second order in the adiabatic perturbation series we thus obtain

$$\begin{aligned} \dot{S}_t &\simeq \beta^{\text{qu}} \dot{Q}_t^{\text{qu}} + \int d\mathbf{z} \left\{ \frac{\beta^{\text{qu}}}{m} (\zeta_x^{\text{qu}} p^2 - D_x^{\text{qu}}) P_t \right. \\ &\quad \left. - \frac{(j_t^{\text{qu}} + j_t^{\text{cl}}) \partial_p P_t}{P_t} \right\}. \end{aligned} \quad (39)$$

Here we have introduced the irreversible probability currents

$$j_t^{\text{qu}} \equiv -\zeta_x^{\text{qu}} p P_t - D_x^{\text{qu}} \partial_p P_t, \quad (40a)$$

$$j_t^{\text{cl}} \equiv -\zeta^{\text{cl}} p P_t - D^{\text{cl}} \partial_p P_t, \quad (40b)$$

and inserted the expression (35a) for the quantum heat current \dot{Q}_t^{qu} . Furthermore, we have used the relation

$$\partial_\alpha \ln Y_\alpha = \mathbb{T}[Y_\alpha] \partial_\alpha Y_\alpha, \quad (41)$$

with the superoperator

$$\mathbb{T}[Y] \circ = \int_0^\infty d\lambda (Y + \lambda)^{-1} \circ (Y + \lambda)^{-1}, \quad (42)$$

which holds for any positive definite matrix Y [118]. Finally, inserting the definitions (40) of the dissipative currents into Eq. (39) gives

$$\dot{S}_t = \beta^{\text{qu}} \dot{Q}_t^{\text{cl}} + \beta^{\text{cl}} \dot{Q}_t^{\text{cl}} + \sigma_t \quad (43)$$

with the total rate of entropy production

$$\sigma_t \equiv \int d\mathbf{z} \left\{ \frac{(j_t^{\text{qu}})^2}{D_x^{\text{qu}} P_t} + \frac{(j_t^{\text{cl}})^2}{D^{\text{cl}} P_t} \right\} \geq 0. \quad (44)$$

This result shows that the heat currents defined in Eq. (35) are consistent with the second law,

$$\sigma_t = \dot{S}_t - \beta^{\text{qu}} \dot{Q}_t^{\text{qu}} - \beta^{\text{cl}} \dot{Q}_t^{\text{cl}} \geq 0. \quad (45)$$

We note that the irreversible currents $j_t^{\text{qu/cl}}$ are zero for $\beta^{\text{cl}} = \beta^{\text{qu}}$ and hence the total rate of entropy production vanishes in equilibrium along with both heat currents, as thermodynamic consistency requires.

B. Stochastic thermodynamics

On the ensemble level, the first and second law are given by Eqs. (33) and (45). With these prerequisites, we are now ready to develop the stochastic thermodynamics of a quantum thermal machine that delivers its output to a classical load. To this end, we consider the quantum and classical subsystems, respectively, as the working medium and load of such a machine. Input is provided in the form of thermal energy from a heat source that periodically modulates the temperature of the quantum reservoir R_{qu} .

Upon assuming that the motion of the classical degree of freedom can be continuously observed, a stochastic first law can be derived from the expression

$$\mathcal{E}^{\text{qu}}[\mathbf{z}_t, \dot{\mathbf{z}}_t] \equiv \mathcal{E}_t^{\text{qu}} = \text{Tr}[H_{x_t}^{\text{qu}} \rho_t] \quad (46)$$

for the trajectory-resolved internal energy of the working medium, i.e., the quantum subsystem. We recall that the density matrix of the quantum subsystem ρ_t is given by Eq. (11) and is thus a function of the classical phase-space variables and their time derivatives. Upon taking a time derivative of Eq. (46) and neglecting third-order corrections in the adiabatic-response expansion, we obtain the balance equation

$$\begin{aligned} \dot{\mathcal{E}}_t^{\text{qu}} &= -\text{Tr}[F_{x_t} \rho_t] p_t/m + \text{Tr}[H_{x_t}^{\text{qu}} \dot{\rho}_t] \\ &= \mathcal{F}'_{x_t} p_t/m + \zeta_t^{\text{qu}} p_t^2/m + \text{Tr}[H_{x_t}^{\text{qu}} \mathcal{L}_{x_t} \rho_t] \\ &\equiv \dot{w}_t + \dot{q}_t^{\text{ex}} + \dot{q}_t^{\text{d}}, \end{aligned} \quad (47)$$

with

$$\dot{w}_t = \mathcal{F}'_{x_t} p_t/m, \quad \dot{q}_t^{\text{ex}} = \zeta_t^{\text{qu}} p_t^2/m, \quad \dot{q}_t^{\text{d}} = \text{Tr}[H_{x_t}^{\text{qu}} \mathcal{L}_{x_t} \rho_t]. \quad (48)$$

Here, we have identified \dot{w}_t as the rate at which work is performed on the quantum system by the classical one along a given trajectory \mathbf{z}_t and \dot{q}_t^{d} denotes the associated heat flux from the quantum reservoir into the working medium. The quantity \dot{q}_t^{ex} must then correspond to the rate at which heat is dissipated from the classical subsystem into the quantum one.

To determine the efficiency of the machine, we have to analyze its entropy balance, which can be developed by identifying the trajectory-resolved entropy of the quantum subsystem as

$$\mathcal{S}^{\text{qu}}[\mathbf{z}_t, \dot{\mathbf{z}}_t] \equiv \mathcal{S}_t^{\text{qu}} = -\text{Tr}[\rho_t \ln \rho_t]. \quad (49)$$

Taking a time derivative of this quantity and neglecting third-order corrections leaves us with

$$\dot{\mathcal{S}}_t^{\text{qu}} = -\text{Tr}[(\mathcal{L}_{x_t} \rho_t) \ln \rho_t] \quad (50)$$

$$= \text{Tr}[(\mathcal{L}_{x_t} \rho_t)(\ln \varrho_{x_t}^{\text{qu}} - \ln \rho_t)] + \beta^{\text{qu}} \dot{q}_t^{\text{d}} \quad (51)$$

where $\varrho_{x_t}^{\text{qu}}$ is the instantaneous Gibbs state of the quantum subsystem defined in Eq. (7). Since $\mathcal{L}_x \varrho_x^{\text{qu}} = 0$, the first term in the second line is non-negative by Spohn's theorem [119]. For fixed β^{qu} , we therefore have

$$\dot{\mathcal{S}}_t^{\text{qu}} - \beta^{\text{qu}} \dot{q}_t^{\text{d}} \geq 0. \quad (52)$$

We now assume that the quantum-classical system is driven into a periodic state by cyclic modulations of the temperature of the quantum reservoir. For the sake of concreteness we focus on a two-stroke engine cycle, whereby the inverse temperature of the quantum reservoir switches periodically between two values β_h^{qu} and $\beta_c^{\text{qu}} > \beta_h^{\text{qu}}$. The switching takes place at the time $0 < t_s < \tau$ where τ denotes the period of the cycle. Up to a short time interval immediately after each temperature switch, where the quantum subsystem is no longer close to its instantaneous equilibrium state, our adiabatic response approach is then applicable in each individual stroke. Furthermore, any corrections to the dissipated heat that arise from the relaxation processes between the strokes can be consistently evaluated as a difference between instantaneous equilibrium energies, as long as the temperature gradient is sufficiently small [37]. That is, the accumulated stochastic work and heat contributions for one cycle are given by

$$w = \int_0^\tau dt \dot{w}_t, \quad q^{\text{ex}} = \int_0^\tau dt \dot{q}_t^{\text{ex}}, \quad q^{\text{d}} = q_h^{\text{d}} + q_c^{\text{d}}, \quad (53)$$

where

$$q_h^{\text{d}} = \int_0^{t_s} dt \dot{q}_t^{\text{d}} + \varepsilon_{x,0}, \quad q_c^{\text{d}} = \int_{t_s}^\tau dt \dot{q}_t^{\text{d}} + \varepsilon_{x,t_s} \quad (54)$$

and

$$\varepsilon_{x,t} = \lim_{\epsilon \rightarrow 0} \left(\text{Tr}[H_{x,t+\epsilon}^{\text{qu}} \varrho_{x,t+\epsilon}^{\text{qu}}] - \text{Tr}[H_{x,t-\epsilon}^{\text{qu}} \varrho_{x,t-\epsilon}^{\text{qu}}] \right) \quad (55)$$

account for the heat that is dissipated while the quantum subsystem returns to its adiabatic-response state right after the temperature switches.

Integrating the first and second law, Eqs. (47) and (50), over a full period therefore provides the relations

$$\mathcal{E}_\tau^{\text{qu}} - \mathcal{E}_0^{\text{qu}} = w + q^{\text{d}} + q^{\text{ex}}, \quad (56a)$$

$$\mathcal{S}_\tau^{\text{qu}} - \mathcal{S}_0^{\text{qu}} \geq \beta_h^{\text{qu}} q_h^{\text{d}} + \beta_c^{\text{qu}} q_c^{\text{d}}, \quad (56b)$$

where the differences on the left do not vanish in general, even though the system is in a periodic state, since \mathcal{E}^{qu} and \mathcal{S}^{qu} are stochastic variables. After taking the ensemble average, however, we are left with

$$0 = W + Q_h^{\text{ex}} + Q_c^{\text{ex}} + Q_h^{\text{d}} + Q_c^{\text{d}}, \quad (57a)$$

$$0 \geq \beta_h^{\text{qu}} Q_h^{\text{d}} + \beta_c^{\text{qu}} Q_c^{\text{d}}. \quad (57b)$$

Here,

$$W = \int_0^\tau dt \int d\mathbf{z} \mathcal{F}'_x p P_t/m, \quad (58)$$

corresponds to the average work that is delivered to the classical degree of freedom per cycle and

$$Q_h^{\text{ex}} = \int_0^{t_s} dt \int d\mathbf{z} \zeta_x^{\text{qu}} p^2 P_t/m, \quad (59a)$$

$$Q_h^{\text{d}} = \int_0^{t_s} dt \int d\mathbf{z} \text{Tr}[H_x^{\text{qu}} \mathcal{L}_x \rho_{\mathbf{z},t}] + \int d\mathbf{z} \varepsilon_{x,0}, \quad (59b)$$

denote the mean heat exchange between working system and load and the mean heat uptake from the quantum reservoir during the hot phase of the cycle, respectively; the corresponding quantities Q_c^{ex} and Q_c^{d} for the cold stroke are defined analogously. The efficiency of the engine can now be consistently defined as

$$\eta = -W/Q_h^{\text{d}} \leq 1 + Q_c^{\text{d}}/Q_h^{\text{d}} \leq \eta_C \quad (60)$$

where the upper bound $\eta_C = \beta_h^{\text{qu}}/\beta_c^{\text{qu}}$, which corresponds to the Carnot value, follows directly from the relations (57) and by noting that $Q_h^{\text{ex}}, Q_c^{\text{ex}} \geq 0$, as becomes evident from Eq. (59a), since ζ_x^{qu} and P_t are both non-negative.

IV. QUANTUM-CLASSICAL RYDBERG SYSTEM

After developing our general framework, we will now show how it can be applied to a concrete model of a heat engine based on an opto-mechanical setup. We first outline the physical setup and then develop its mathematical description with the help of suitable approximations. Specifically, we will consider two examples of thermodynamic processes, a single-stroke expansion and a two-stroke cycle. We then analyze the statistics of thermodynamic quantities such as work and heat and calculate the efficiency of the two-stroke engine by means of numerical simulations.

A. System

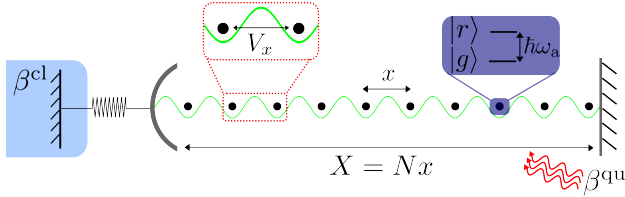


FIG. 2. Schematic of our quantum-classical engine. The working system consists of a chain of N Rydberg atoms, which sit at the minima of a standing light wave inside an optical cavity. The atoms are modelled as two-level systems and are equally spaced by a distance x , which effectively plays the role of the classical degree of freedom. The cavity length is $X = Nx$. The atoms interact via a dipole-dipole interaction, described by the potential V_x and are driven by a noisy laser that mimics a thermal reservoir with inverse temperature β^{qu} . The classical work load consists of a movable mirror, which is coupled to a classical bath with inverse temperature β^{cl} . The motion of the mirror is driven by the radiation pressure inside the cavity, which depends on the state of the atoms and the restoring force of a classical spring with constant c .

We consider the hybrid engine shown in Fig. 2. A chain of N interacting Rydberg atoms are confined in an optical cavity by a lattice potential created by a standing

light wave. Each Rydberg atom is treated as a two-level system (TLS), with ground state $|g\rangle$ and excited Rydberg state $|r\rangle$. We assume that the two levels are coupled by a noisy laser, so that quantum superpositions between the two states decohere quickly. State changes within the atoms can thus be described by a rate equation. The noisy laser plays the role of a thermal reservoir, and can be modelled as an ensemble of non-interacting bosons at inverse temperature β^{qu} [120]. The free evolution of the Rydberg chain is described by the Hamiltonian

$$H_x^{\text{qu}} = \hbar\omega_a \sum_{k=1}^N n_k + V_x \sum_{k=1}^{N-1} n_k n_{k+1}, \quad (61)$$

where $n_k = |r_k\rangle\langle r_k|$ and the atoms experience nearest neighbour dipole-dipole interactions $V_x = v/x^3$, which depend on their separation x . The cavity is formed by a fixed mirror and a movable mirror of mass m , which is in contact with a classical reservoir with inverse temperature β^{cl} . The position of the movable mirror plays the role of the classical degree of freedom, $X_t = Nx_t$, and determines the size of the cavity and thus the length of the standing light wave that confines the atomic array. That is, we assume that the atoms sit at the minima of the trapping potential and are therefore evenly spaced along the cavity.

The quantum and classical subsystems interact with each other through the radiation pressure inside the cavity, which effectively arises from the interactions between neighbouring atoms. The resulting force on the movable mirror is counterbalanced by the restoring force of a classical spring

$$-\partial_X U_X = -c(X - X_0), \quad (62)$$

with spring constant c , which pushes the mirror to its natural position X_0 .

B. Model

1. Quantum Dynamics

The state of the quantum system ρ_t evolves under a collective many-body master equation,

$$\dot{\rho}_t = \mathcal{L}_x \rho_t \equiv \mathcal{H}_x \rho_t + \mathcal{D}_x \rho_t, \quad (63)$$

where

$$\begin{aligned} \mathcal{H}_x \circ &= -\frac{i}{\hbar} [\circ, H_x^{\text{qu}}] \quad \text{and} \\ \mathcal{D}_x \circ &= \sum_{k=1}^N \sum_{\alpha=0}^2 \left\{ \chi_x^{\alpha-} \mathcal{K}[J_k^{\alpha}] \circ + \chi_x^{\alpha+} \mathcal{K}[J_k^{\alpha\dagger}] \circ \right\} \end{aligned} \quad (64)$$

denote the Liouville and dissipative super-operators and $\mathcal{K}[Y]$ is defined in Eq. (4). The energy of emitted and absorbed photons from a particular atom depend on the

state of the neighbouring atoms in the chain, owing to the nearest neighbour interaction [121]. The collective jump operators that describe this effect are given by

$$J_k^\alpha = \begin{cases} \tilde{n}_{k-1}\sigma_k^- \tilde{n}_{k+1} & \alpha = 2 \\ (\mathbb{I}_k - \tilde{n}_{k-1})\sigma_k^- \tilde{n}_{k+1} & \alpha = 1 \\ \quad + \tilde{n}_{k-1}\sigma_k^- (\mathbb{I}_k - \tilde{n}_{k+1}) & \\ (\mathbb{I}_k - \tilde{n}_{k-1})\sigma_k^- (\mathbb{I}_k - \tilde{n}_{k+1}) & \alpha = 0 \end{cases}, \quad (65)$$

with $\tilde{n}_{k-1} \equiv n_{k-1}(1 - \delta_{k-1})$ and $\tilde{n}_{k+1} \equiv n_{k+1}(1 - \delta_{k-N})$. Since we consider open boundary conditions, only the jump operators with $\alpha \leq 1$ are defined at the ends of the chain, i.e., for $k = 1$ and $k = N$. Furthermore,

$$\mathbb{I}_k = n_k + g_k \quad \text{with} \quad g_k = |g_k\rangle\langle g_k| \quad (66)$$

denotes the single-atom identity matrix. The resulting Bohr frequencies account for the number of excited atoms α in the neighbourhood of the k -th atom and read

$$\nu_{x,\alpha} = \omega_a + \alpha V_x / \hbar. \quad (67)$$

The corresponding collective decay rates are

$$\chi_x^{\alpha+} = \gamma_{x,\alpha} \mathcal{B}_{x,\alpha} \quad \text{and} \quad \chi_x^{\alpha-} = \gamma_{x,\alpha} (\mathcal{B}_{x,\alpha} + 1), \quad (68)$$

where $\gamma_{x,\alpha} = 2\pi\hbar\kappa\nu_{x,\alpha}^3$. The constant κ sets the scale of the decay rates and the Bose-Einstein distribution

$$\mathcal{B}_{x,\alpha} = (\exp[\beta^{\text{qu}}\hbar\nu_{x,\alpha}] - 1)^{-1} \quad (69)$$

describes the effective reservoir mimicked by the noisy laser. Thus, the collective decay rates obey the detailed balance condition

$$\chi_x^{\alpha+} / \chi_x^{\alpha-} = \exp[-\beta^{\text{qu}}\hbar\nu_{x,\alpha}] \quad (70)$$

and the unique stationary solution of the master equation (63) is the Gibbs state

$$\varrho_x^{\text{qu}} = \exp[-\beta^{\text{qu}}(H_x^{\text{qu}} - \mathcal{F}_x)], \quad (71)$$

where

$$\mathcal{F}_x \equiv -\ln \text{Tr}[\exp[-\beta^{\text{qu}}H_x^{\text{qu}}]] / \beta^{\text{qu}} \quad (72)$$

is the free energy of the quantum system. The non-local master equation (63) has been derived following the approach taken in Ref. [121], and adapting it to allow for a finite reservoir temperature.

2. Classical dynamics

The classical equations of motion are the Langevin equations

$$\dot{X}_t = Np_t/m, \quad (73a)$$

$$N\dot{p}_t = -\partial_{X_t}U_{X_t} + f_{\mathbf{z},t}^{\text{qu}} - N\zeta^{\text{cl}}p_t + \xi_t^{\text{cl}}, \quad (73b)$$

where p_t is the momentum of a single atom of the chain and $f_{\mathbf{z}}^{\text{qu}}$ is the quantum coupling force. Since the position of the movable mirror is linearly dependent on the interatomic spacing we can, upon rescaling with the atom number N , replace the cavity length X with the spacing between atoms x as our classical degree of freedom. The logic behind this rescaling is two-fold. First, since the atoms are evenly spaced inside the cavity, working with the interatomic spacing will allow us to apply the equations of motion for an arbitrary number of atoms, where we have an equilibrium spacing $x_0 = X_0/N$ corresponding to an experimentally feasible value. That is, we increase the equilibrium length of the cavity proportional to the number of atoms so that an infinite density scenario, where the spacing between atoms inside the cavity becomes unfeasibly small, is avoided. Second, the Hamiltonian of the quantum system and the generator of the master equation that describes its time evolution depend only on the interatomic spacing and so rescaling allows us to consistently work with a single classical degree of freedom. The time evolution of the spacing is governed by the Langevin equation

$$\dot{x}_t = p_t/m, \quad (74a)$$

$$\dot{p}_t = -U'_t + f_{\mathbf{z},t}^{\text{qu}}/N - \zeta^{\text{cl}}p_t + \xi_t^{\text{cl}}/N, \quad (74b)$$

where the restoring force of the movable mirror is now

$$-U'_x = -c(x - x_0) \quad (75)$$

with primes denoting partial derivatives with respect to x . The classical diffusion constant D^{cl} enters upon inserting the fluctuation-dissipation relation (10) and the classical stochastic force ξ_t^{cl} obeys the relations (9).

The quantum coupling force per particle,

$$f_{\mathbf{z},t}^{\text{qu}}/N = -\mathcal{F}'_x/N^2 - \zeta_x^{\text{qu}}p + \xi_{x,t}^{\text{qu}}/N, \quad (76)$$

consists of the deterministic force per particle \mathcal{F}'_x/N^2 and the friction term $\zeta_x^{\text{qu}}p = \beta^{\text{qu}}D_x^{\text{qu}}p/m$, where the associated diffusion constant is given by

$$D_x^{\text{qu}} = -\langle\langle (\mathbb{L}_x^\dagger)^{-1} \delta F_x; \delta F_x \rangle\rangle_{\varrho_x^{\text{qu}}}, \quad (77)$$

with

$$\delta F_x = -\frac{V'_x}{N} \left(\sum_{k=1}^N n_k n_{k+1} - \text{Tr} \left[\sum_{k=1}^N n_k n_{k+1} \varrho_x^{\text{qu}} \right] \right) \quad (78)$$

for the Rydberg chain. The stochastic contribution describes the noise induced by the quantum subsystem and is related to the diffusion constant D_x^{qu} by Eq. (16).

C. Mean-field approximation

Obtaining analytic expressions for the quantum coupling force is in general not straightforward for a many-body system. In particular, owing to the collective nature of the master equation (63), where jump rates and

operators for individual atoms depend on their immediate neighbourhood, the diffusion constant (77) would have to be determined numerically, which is possible only for small values of N . To calculate mean-values of few body observables, however, we do not necessarily need to resolve the neighbourhood of each individual atom. Instead, we may assume that the interaction between neighbouring atoms induces, on average, a homogeneous energy shift. This assumption is justified if the scale of thermal fluctuations is large relative to the scale of the inter-atomic interactions, i.e. if $\beta^{\text{qu}} V_x \ll 1$ and if the number of atoms is sufficiently large so that individual local excitations have only a negligible effect on average quantities. If these conditions are met, we can proceed with a mean-field (MF) approach, where the nearest neighbour excitation operators $n_{k\pm 1}$ in the collective master equation (63) are replaced with the average excitation density

$$\langle n_x \rangle = \frac{1}{N} \text{Tr} \left[\sum_{k=1}^N n_k \varrho_x^{\text{qu}} \right] \equiv \frac{1}{N} \partial_{\hbar\omega_a} \mathcal{F}_x. \quad (79)$$

The MF master equation thus becomes

$$\dot{\rho}_t = \bar{\mathcal{L}}_x \rho_t \equiv \mathbf{H}_x \rho_t + \bar{\mathbf{D}}_x \rho_t, \quad (80)$$

where

$$\bar{\mathbf{D}}_x \circ = \sum_{k=1}^N \left\{ \bar{\chi}_{x,k}^- \mathbf{K}[\sigma_k^-] \circ + \bar{\chi}_{x,k}^+ \mathbf{K}[\sigma_k^+] \circ \right\}, \quad (81)$$

and we use bars to denote MF quantities throughout. The MF rates reflect the collective nature of decay and excitation and are given by

$$\bar{\chi}_{x,k}^{\pm} = \begin{cases} \langle n \rangle^2 \chi^{1\pm} + (1 - \langle n \rangle)^2 \chi^{0\pm} & \text{if } k = 1 \text{ or } N \\ \langle n \rangle^4 \chi^{2\pm} + 4\langle n \rangle^2 (1 - \langle n \rangle)^2 \chi^{1\pm} \\ \quad + (1 - \langle n \rangle)^4 \chi^{0\pm} & \text{otherwise} \end{cases}, \quad (82)$$

We note that, for notational convenience, we drop the x -dependence of the collective rates $\bar{\chi}^{\alpha\pm}$ and the excitation density $\langle n \rangle$ from here onwards. The unique stationary solution of the master equation (80) is given by the product state

$$\bar{\varrho}_x^{\text{qu}} = \bigotimes_{k=1}^N (\bar{\chi}_{x,k}^+ n_k + \bar{\chi}_{x,k}^- g_k) / \bar{\chi}_{x,k}^N, \quad \text{with } \bar{\chi} = \bar{\chi}^- + \bar{\chi}^+, \quad (83)$$

which approximates the thermal state of the quantum subsystem in the parameter regimes, where the MF approximation is valid.

In addition we now replace open with periodic boundary conditions. Although our physical setup in principle requires open boundary conditions, this approximation, which enhances the transparency of our mathematical model, is still justified for sufficiently large chains, where boundary effects play only a minor role. The MF decay rates then become independent of k and are given by

$$\bar{\chi}_x^{\pm} = \langle n \rangle^4 \chi^{2\pm} + 4\langle n \rangle^2 (1 - \langle n \rangle)^2 \chi^{1\pm} + (1 - \langle n \rangle)^4 \chi^{0\pm}. \quad (84)$$

With these simplifications, it becomes possible to explicitly calculate the terms that appear in the second-order adiabatic-response approximation (11). Specifically, the state of the quantum subsystem is given by

$$\bar{\rho}_t = \bar{\varrho}_t^{\text{qu}} + \bar{\rho}_t^{(x)} p_t + \bar{\rho}_t^{(2x)} p_t^2 + \bar{\rho}_t^{(p)} \dot{p}_t, \quad (85)$$

where

$$\begin{aligned} \bar{\rho}_x^{(x)} &= \frac{1}{Nm} \bar{\mathcal{L}}_x^{-1} \bar{\varrho}_x^{\text{qu}'}, \quad \bar{\rho}_x^{(2x)} = \frac{1}{N^2 m} \bar{\mathcal{L}}_x^{-1} \bar{\rho}_x^{(x)'}, \\ \bar{\rho}_x^{(p)} &= \bar{\mathcal{L}}_x^{-1} \bar{\rho}_x^{(x)}, \end{aligned} \quad (86)$$

and the derivative of the MF steady state is

$$\bar{\varrho}_x^{\text{qu}'} = \frac{\bar{\chi}_x^-}{\bar{\chi}_x^+} \delta \bar{F}_x^{\hbar\omega_a} \bar{\varrho}_x^{\text{qu}} \partial_x \left(\frac{\bar{\chi}_x^+}{\bar{\chi}_x^-} \right), \quad (87)$$

with $\delta \bar{F}_x^{\hbar\omega_a} = -\partial_{\hbar\omega_a} H_x^{\text{qu}} + \text{Tr}[\partial_{\hbar\omega_a} H_x^{\text{qu}} \bar{\varrho}_{\text{qu}}]$.

1. MF quantum coupling force

The terms that appear in the expression (76) for the quantum force can now be determined in the MF picture. The deterministic force contribution is given by

$$\bar{\mathcal{F}}_x' / N = \text{Tr}[H_x^{\text{qu}'} \bar{\varrho}_x^{\text{qu}}] / N = V_x' \left(\frac{\bar{\chi}_x^+}{\bar{\chi}_x^-} \right)^2. \quad (88)$$

This expression is independent of N as expected since in the rescaled picture the cavity length increases with the number of atoms and the relative interatomic spacing is unchanged. The systematic force that the quantum system exerts on the mirror therefore remains unchanged with the number of atoms in the chain.

The quantum diffusion constant, involves the adjoint Lindblad super-operator and in the MF picture becomes

$$\bar{D}_x^{\text{qu}} = -\langle\langle (\bar{\mathcal{L}}_x^{\dagger})^{-1} \delta \bar{F}_x; \delta \bar{F}_x \rangle\rangle_{\bar{\varrho}^{\text{qu}}}, \quad (89)$$

where $\delta \bar{F}_x = F_x + \bar{\mathcal{F}}_x'$ and

$$\bar{\mathcal{L}}_x^{\dagger} \circ \equiv \mathbf{H}_x \circ + \sum_{k=1}^N \left(\bar{\chi}^+ \mathbf{K}^{\dagger}[\sigma_k^+] \circ + \bar{\chi}^- \mathbf{K}^{\dagger}[\sigma_k^-] \circ \right) \quad (90)$$

with

$$\mathbf{K}^{\dagger}[Y] \circ = Y^{\dagger} \circ Y - Y^{\dagger} Y \circ / 2 - \circ Y^{\dagger} Y / 2. \quad (91)$$

This expression can be evaluated explicitly, which yields the result

$$\bar{D}_x^{\text{qu}} = V_x'^2 \frac{\bar{\chi}_x^{+2} \bar{\chi}_x^- (8\bar{\chi}_x^+ + \bar{\chi}_x^-)}{2N\bar{\chi}_x^5}, \quad (92)$$

for details see App. A 1. We recall that the quantum diffusion constant is related to the MF quantum noise through the relation

$$\langle \bar{\xi}_{x,t}^{\text{qu}} \bar{\xi}_{x,t'}^{\text{qu}} \rangle = 2\bar{D}_x^{\text{qu}} \delta_{t-t'}. \quad (93)$$

Thus the Langevin equations that describe the dynamics of the effective classical degree of freedom become

$$\dot{x}_t = p_t/m, \quad (94a)$$

$$\dot{p}_t = -c(x_t - x_0) - \bar{\mathcal{F}}'_t/N^2 - (\beta^{\text{qu}}\bar{D}_t^{\text{qu}} + \beta^{\text{cl}}D^{\text{cl}})\dot{x}_t + \xi_t^{\text{cl}}/N + \bar{\xi}_t^{\text{qu}}/N, \quad (94b)$$

where all quantities are known explicitly and $\bar{\mathcal{F}}'$ and \bar{D}^{qu} depend only on time through x_t . We therefore have derived a full dynamical description of our quantum-classical engine in the MF picture.

D. Thermodynamic processes

We are now ready to explore the stochastic thermodynamics of our quantum-classical hybrid machine. We first observe that, within the mean-field picture, the rates of work applied to the classical load, heat exchange with the quantum working system and heat uptake from the quantum reservoir, per particle, are given by

$$\dot{w}_t = V'_t \left(\frac{\bar{\chi}_t^+}{\bar{\chi}_t} \right)^2 \dot{x}_t \quad (95a)$$

$$\dot{q}_t^{\text{ex}} = \beta^{\text{qu}} V_t'^2 \frac{\bar{\chi}_t^{+2} \bar{\chi}_t^- (8\bar{\chi}_t^+ + \bar{\chi}_t^-)}{2N\bar{\chi}_t^5} \dot{x}_t^2, \quad (95b)$$

$$\dot{q}_t^{\text{d}} = \text{Tr}[H_t^{\text{qu}} \bar{\mathcal{L}}_t \bar{\rho}_t^{(x)}] p_t + \text{Tr}[H_t^{\text{qu}} \bar{\mathcal{L}}_t \bar{\rho}_t^{(p)}] \dot{p}_t + \text{Tr}[H_t^{\text{qu}} \bar{\mathcal{L}}_t \bar{\rho}_t^{(2x)}] p_t^2, \quad (95c)$$

respectively, where we provide the explicit result for \dot{q}_t^{d} in App. A 2. These expressions are obtained by inserting the mean-field approximations (85)-(88) into the general formulas (48). As we will show in the following, they make it possible to infer the full distributions of thermodynamic quantities on the level of single trajectories from numerical simulations of the Langevin equations (94).

We consider two examples of thermodynamic processes: a single stroke expansion of the cavity and a two-stroke engine cycle. The Langevin dynamics described by Eq. (94), is simulated using an Euler-Maruyama method, which we explain further in App. B. Throughout this section we consider a chain with $N = 100$ Rydberg atoms. The interaction strength between nearest-neighbour atoms is $V_x = v/x^3$ where we choose $v = 5\hbar\omega_a x_0^3$ as is typical for the baseline interaction strength of trapped Rydberg atoms [122]. We also fix the spring constant, the classical diffusion constant and the inverse temperature of the classical reservoir at $c = \hbar\omega_a/x_0^2$, $D^{\text{cl}} = 10^5 \hbar^2 \omega_a/x_0$ and $\beta^{\text{cl}} = 0.1/\hbar\omega_a$. Since all relevant thermodynamic quantities are linear in N within the mean-field picture, we will only consider work and heat contributions per atom in the chain.

1. Single-stroke expansion

The single-stroke expansion is illustrated in Fig. 3a). We consider the movable mirror to be fixed at an initial position $X_i \equiv X_0$, equal to its natural resting position in the absence of any radiation pressure inside the cavity, i.e., for $\beta^{\text{qu}} = \infty$ and $\bar{\mathcal{F}}'_x = 0$. Upon turning on the noisy laser, the atoms in the chain are exposed to an effective environment with inverse temperature $\beta^{\text{qu}} > 0$ which leads to a rise in radiation pressure and thus a non-zero quantum coupling force. As a result, once the mirror is released, the cavity expands and the mirror settles, on average, to a new equilibrium position X_f .

We plot the average position of the mirror together with exemplary single trajectories in Fig. 3b. The larger the effective temperature of the quantum reservoir, the further the mirror is pushed by the cavity and the more its final equilibrium position X_f deviates from its initial position X_0 . The total work done by the quantum system on the movable mirror during the expansion is given by

$$w_{\text{sse}} = \int_0^t dt \dot{w}_t \quad (96)$$

where t has to be chosen sufficiently large such that the mirror has reached its new equilibrium position. Fig. 3b indicates that no systematic motion of the mirror occurs anymore after $t = 10^6 \omega_a^{-1}$; we therefore set $t = 2 \times 10^6 \omega_a^{-1}$ in the following. In part (c) of Fig. 3 we plot the rescaled potential $u_x = c(x - x_0)^2/2 + \bar{\mathcal{F}}_x/N^2$, which is responsible for the average final resting position of the mirror. Since we obtain the time-resolved position x_t of the mirror from our simulation of the Langevin equation (94), we can now calculate w_{sse} for any individual trajectory. Upon repeating this simulation sufficiently many times, we can determine the distribution of this quantity, which is given by

$$P(w_{\text{sse}}) = \frac{1}{M} \sum_{m=1}^M \Pi_\epsilon[w_{\text{sse}} - w_{\text{sse}}^{(m)}], \quad (97)$$

for sufficiently large M , where $w_{\text{sse}}^{(m)}$ is the work performed along the m -th trajectory and

$$\Pi_\epsilon[x] = \begin{cases} 1 & \text{if } -\epsilon/2 \leq x \leq \epsilon/2 \\ 0 & \text{otherwise} \end{cases} \quad (98)$$

is a boxcar function with width ϵ . The distributions are plotted in part (d) of Fig. 3. These plots show nearly Gaussian distributions with a slight asymmetry. Their mean value depends on the inverse temperature of the quantum bath, which determines the radiation pressure inside the cavity. In addition, we observe that the width of the work distributions increases with the temperature of the quantum reservoir, due to enhanced thermal fluctuations.

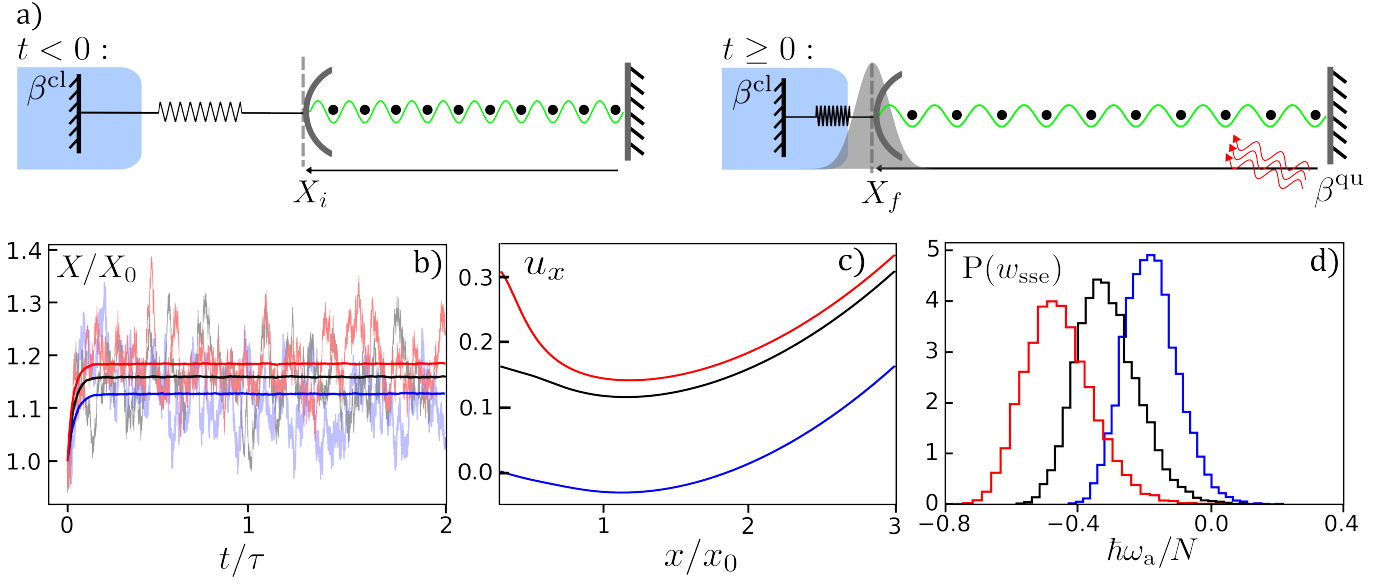


FIG. 3. a) Schematic outline of a single-stroke expansion. For $t < 0$, the movable mirror is held at some initial position X_i . At $t = 0$, the mirror is released and the cavity expands under the internal radiation pressure, generated by the quantum system, which is coupled to a noisy laser playing the role of a thermal bath with inverse temperature β^{qu} . b) Plots of the average mirror position and individual trajectories over time, shown for three different inverse temperatures of the quantum bath, $\beta^{\text{qu}} = \beta^{\text{cl}}$ (blue), $0.5\beta^{\text{cl}}$ (black) and $0.1\beta^{\text{cl}}$ (red). The time scale over which the expansion takes place is $\tau = 2 \times 10^6 \omega_a^{-1}$. c) The rescaled effective potential $u_x = \frac{1}{2}c(x - x_0)^2 + \mathcal{F}_x/N^2$ acting on the classical degree of freedom for the same temperatures as in b). d) Histograms of the work distribution for 10^4 realizations of the same single-stroke expansions in b).

2. Two-Stroke engine cycle

As our second example, we consider a two-stroke engine cycle with the quantum system acting as the working medium. The engine cycle is realized by periodic modulation of the external laser field, so that the effective inverse temperature of the quantum reservoir oscillates between the two values $\beta_c^{\text{qu}} \equiv \beta^{\text{cl}}$ and $\beta_h^{\text{qu}} < \beta_c^{\text{qu}}$. The process is outlined in Fig. 4a. In the first stroke, where $0 \leq t < \tau/2$, the cavity expands under the increased radiation pressure induced by the quantum reservoir at β_h^{qu} . In the second stroke, where $\tau/2 \leq t < \tau$, the laser intensity is adjusted to emulate the cold quantum bath with β_c^{qu} , so that the movable mirror of the cavity relaxes to a new position. The period of the cycle is $\tau = 2 \times 10^6 \omega_a^{-1}$ so that the adiabatic-response assumption is justified within the individual strokes, except for minor corrections incurred right after the switching of the temperature. That is, the quantum system quickly relaxes to its new adiabatic-response state after the external field changes at the start of each stroke. Here the temperature difference between the hot and cold stroke must also be small relative to the internal energy scale of the quantum system in order for the thermodynamics of a two-stroke cycle to be consistently described by the adiabatic response framework without introducing a systematic expansion in $\Delta\beta^{\text{qu}} = \beta_h^{\text{qu}} - \beta_c^{\text{qu}}$ [37].

We simulate the position of the movable mirror over 5 cycles, and average over 10^4 trajectories in Fig. 4b. We find that the mirror settles into a periodic steady state,

within approximately two cycles. Once the engine has relaxed into a periodic steady state we can calculate its accumulated net output over C cycles,

$$w_{\text{tse}}(C) = \int_t^{t+C\tau} dt' \dot{w}_{t'}. \quad (99)$$

In part (c) of Fig. 4 we show three plots for the work distributions for $C = 5, 20$ and 50 cycles. The inset shows that both the mean value and variance of these distributions grow linearly in C , as one would expect. As a second quantity of interest, we consider the heat uptake from the effective quantum reservoir in one cycle q_h^{d} , for different temperature ratios, $\beta_r = \beta_h^{\text{qu}}/\beta_c^{\text{qu}}$. Following the stochastic expression in Eq. (54), the heat uptake in the hot stroke is given by

$$q_h^{\text{d}} = \int_t^{t+\tau} dt' \theta_{t'}^h \dot{q}_{t'}^{\text{d}} + \varepsilon_{x,t_h}, \quad (100)$$

where θ_t^h is 1 during the hot phase of the cycle and zero otherwise and t_h is the time at which the quantum reservoir switches from cold to hot. For our Rydberg engine we take \dot{q}_t^{d} from Eq. (95c) and the contribution from switching the temperature at the start of the stroke is

$$\varepsilon_{x,t_h} = \lim_{\epsilon \rightarrow 0} \left(\frac{\bar{X}_{t_h+\epsilon}^+}{\bar{X}_{t_h+\epsilon}} \left(\hbar\omega_a + V_{t_h+\epsilon} \frac{\bar{X}_{t_h+\epsilon}^+}{\bar{X}_{t_h+\epsilon}} \right) - \frac{\bar{X}_{t_h-\epsilon}^+}{\bar{X}_{t_h-\epsilon}} \left(\hbar\omega_a + V_{t_h-\epsilon} \frac{\bar{X}_{t_h-\epsilon}^+}{\bar{X}_{t_h-\epsilon}} \right) \right) \quad (101)$$

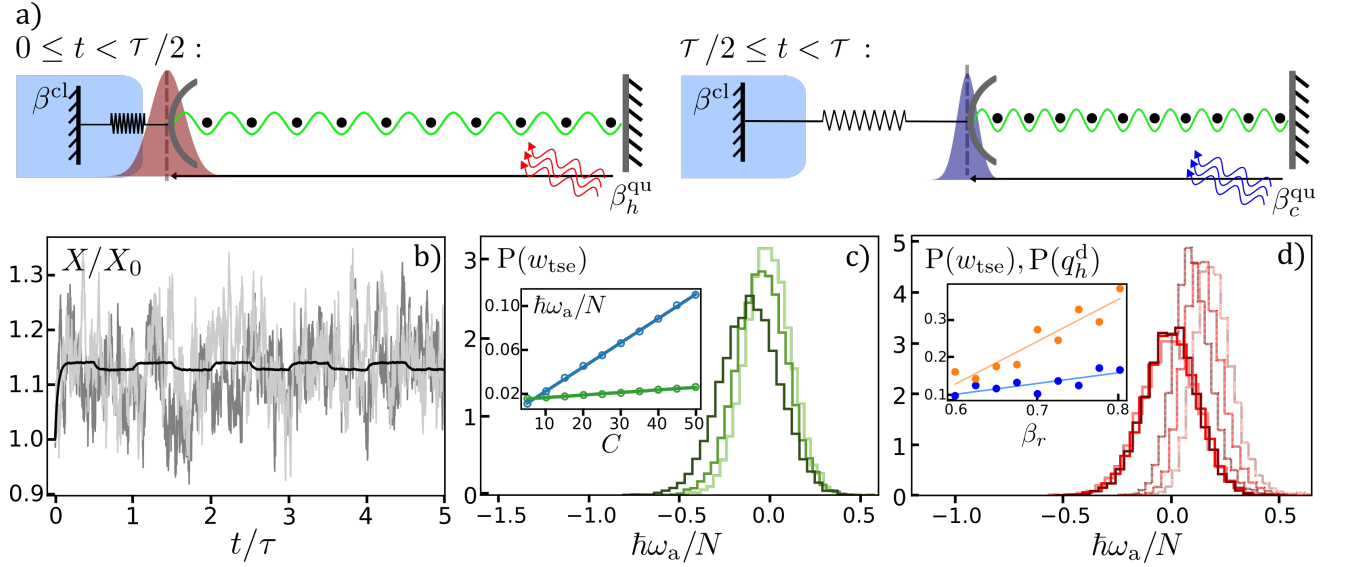


FIG. 4. a) Schematic outline of a two-stroke cycle, driven by periodic temperature modulations. b) Average position of the mirror taken over 10^4 trajectories for 5 cycles (black solid) with $\beta_h^{\text{qu}} = 0.8\beta_c^{\text{cl}}$ and $\beta_c^{\text{qu}} = \beta_c^{\text{cl}}$, $\tau = 2 \times 10^6 \omega_a^{-1}$ fixed throughout all plots. The shaded lines show the position of the mirror from two individual trajectories. c) Plots of the work distribution over $C = 5$ (light green), 20 (green) and 50 (dark green) cycles, with $\beta_h^{\text{qu}} = 0.8\beta_c^{\text{cl}}$. The inset shows the mean W (blue circles) and variance $\text{Var}(W)$ (green circles) of the output work as a function of the number of cycles, ranging from $C = 5 - 50$, with solid lines showing linear fits. d) Distributions of output work w_{tse} (solid) and input heat q_h^d (dotted) for 10^4 realizations of a single cycle, for different values of $\beta_r = \beta_h^{\text{qu}}/\beta_c^{\text{qu}}$. Here β_h^{qu} is changed such that $\beta_r = 0.7$ (brown), 0.75 (red) and 0.8 (pink). The inset shows the corresponding efficiency η (blue) in units of Carnot efficiency η_C as well as the rescaled relative fluctuation of the output work, $\sqrt{\text{Var}(W)}/W^2/100$ (orange), for a range of temperature ratios β_r , with solid lines showing linear fits.

in the MF picture. The corresponding distributions are shown in part (d) of Fig. 4 together with the work distributions for $\beta_r = 0.7, 0.75$ and 0.8 . Finally, from the mean values W and Q_h^d of the output and input distributions, we can calculate the efficiency of our engine $\eta = -W/Q_h^d$, which is plotted in the inset of part (d) of Fig. 4 in units of the Carnot value $\eta_C = 1 - \beta_h^{\text{qu}}/\beta_c^{\text{qu}}$, along with the relative fluctuations of the output work which characterise the stability of the output [123], that is, the constancy of the engine [46]. We find that the efficiency of our engine reaches up to $\sim 18\%$ of the Carnot value. This figure is plausible given that we have not systematically optimized the parameters and driving protocol of our model. We leave this task to future research. The relative work fluctuations are seen to increase with β_r . This behaviour primarily results from the fact that the mean output work decreases with β_r as the mirror's equilibrium positions in the hot and the cold stroke move closer together. In summary, our results demonstrate that the general framework developed in this article makes it possible to obtain the full statistics of thermodynamic processes at the quantum-classical boundary without the necessity of invoking additional measurement protocols, which was our main objective here.

V. PERSPECTIVES

Our case study demonstrates that the essential characteristics of microscopic thermal machines can be realized in quantum-classical hybrid systems. In particular, we have seen that a classical degree of freedom with an observable trajectory provides both a physically intuitive means of work extraction and a powerful tool to infer the statistics of quantum thermodynamic processes. It now remains to find suitable experimental platforms to realize such quantum-classical hybrid engines. In our analysis, we have rescaled the cavity length with $x_0 = 5\mu\text{m}$, which corresponds to the typical inter-particle spacing for trapped Rydberg atoms that can be achieved in current experiments [124]. The magnitudes of the dipole-dipole interactions and the collective decay rates were chosen as $v/x_0^3 = 5\hbar\omega_a$ and $\kappa = 10^{-2}/\hbar\omega_a^2$, where the energy difference between the ground and the Rydberg state was set to the realistic value $\omega_a = 1\text{MHz}$ [122, 124–126]. The mass of the classical degree of freedom scales as $m \propto \hbar/x_0^2\omega_a$, which for our model would lead to a value of the order of $10^{-20}g$. Such a tiny mass cannot be plausibly associated with a nano-mechanical resonator such as a movable mirror. It may, however, be achieved with cold-atoms based opto-mechanical systems, where the mechanical degrees of freedom are formed by collective vibration modes of atomic ensembles [111]. A second avenue towards a more feasible setting could be

to decrease the typical inter-particle distance x_0 , which would lead to an increase in the radiation pressure inside the cavity and thus the force acting on the mirror, as is reflected by the scaling of the effective mass with x_0^{-2} . Overall, our model is meant to conceptualize and illustrate the basic idea and potential benefits of quantum-classical hybrid machines and we leave it to future research to find truly realistic ways of constructing such devices.

On the conceptual side, our framework provides a systematic step towards bridging the long-standing gap between classical stochastic and quantum thermodynamics. Since the concepts of the former theory can be directly applied to the classical degree of freedom, our results lay the ground work for a variety of future research directions, such as the potential formulation of fluctuation theorems and thermodynamic uncertainty relations for quantum-classical hybrid systems or the search for universal trade-off relations between the figures of merit of hybrid thermal machines. In a wider perspective, it would be desirable to extend our approach beyond the limits of the adiabatic-response regime and ultimately to derive a thermodynamically consistent theory of quantum-classical systems from fundamental principles. Useful lessons to this end could be drawn, for instance, from physical chemistry, where hybrid models have long been used to simplify fully quantum descriptions of complex molecular systems [93, 127], from field theory, where the lack of a quantum theory of gravity has long been a driving force for research on quantum-classical dynamics [83, 84], or from mathematical physics, where stochastic descriptions of quantum-classical sys-

tems are currently receiving renewed attention [92, 95–98]. Our thermodynamics-based approach adds a further perspective to this research and might, owing to the universality of thermodynamics as a physical theory, eventually help to unify existing and forthcoming results across different fields.

ACKNOWLEDGMENTS

JE acknowledges support from the German Academic Exchange Service (DAAD). This work was supported by the Medical Research Council (Grants No. MR/S034714/1 and MR/Y003845/1) and the Engineering and Physical Sciences Research Council (Grant No. EP/V031201/1). KB acknowledges insightful discussions with Keiji Saito. FC is indebted to the Baden-Württemberg Stiftung for the financial support by the Eliteprogramme for Postdocs. IL and FC acknowledge funding from the European Union’s Horizon Europe research and innovation program under Grant Agreement No. 101046968 (BRISQ). They also are grateful for financial support through the Deutsche Forschungsgemeinschaft (DFG, German Research Foundation) through the Research Unit FOR 5413/1, Grant No. 465199066. This work was supported by the University of Nottingham and the University of Tübingen’s funding as part of the Excellence Strategy of the German Federal and State Governments, in close collaboration with the University of Nottingham.

Appendix A: Mean-Field Theory

1. Quantum Diffusion constant

We recall the expression

$$D_x^{\text{qu}} = \int_0^\infty dt \langle\langle \delta \hat{F}_{x,t}; \delta \hat{F}_{x,0} \rangle\rangle_{\varrho^{\text{qu}}} \quad (\text{A1})$$

for the quantum diffusion constant, which was defined in Eq. (17). In this appendix, we first show how this quantity can be obtained analytically within the mean-field picture introduced in Sec. IV, and then compare the resulting expression with numerically exact calculations for a small number N of Rydberg atoms.

Within the mean-field approximation, the quantum diffusion constant is given by

$$\bar{D}_x^{\text{qu}} = \int_0^\infty dt \langle\langle \delta \hat{\bar{F}}_{x,t}; \delta \hat{\bar{F}}_{x,0} \rangle\rangle_{\varrho^{\text{qu}}} \quad (\text{A2})$$

where $\delta \hat{\bar{F}}_{x,t}$ denotes the shifted quantum force operator in the Heisenberg picture with respect to the adjoint mean-field generator

$$\bar{\mathcal{L}}_x^\dagger \circ = \mathcal{H}_x \circ + \sum_{k=1}^N \left(\bar{\chi}^+ \mathcal{K}^\dagger [\sigma_k^+] \circ + \bar{\chi}^- \mathcal{K}^\dagger [\sigma_k^-] \circ \right) \quad (\text{A3})$$

with

$$H_x = -\frac{i}{\hbar} [\circ, H_x^{\text{qu}}] \quad \text{and} \quad \mathcal{K}^\dagger[Y] \circ = Y^\dagger \circ Y - Y^\dagger Y \circ / 2 - \circ Y^\dagger Y / 2. \quad (\text{A4})$$

This object satisfies the differential equation

$$\frac{d}{dt} \delta \bar{F}_{x,t} = \bar{\mathcal{L}}_x^\dagger \delta \bar{F}_{x,t} \quad (\text{A5})$$

within respect to the initial condition

$$\delta \bar{F}_{x,0} = F_x + \bar{\mathcal{F}}_{x,t} = -V'_x \left(\sum_{k=1}^N n_k n_{k+1} - \text{Tr} \left[\sum_{k=1}^N n_k n_{k+1} \bar{\varrho}_x^{\text{qu}} \right] \right) / N, \quad (\text{A6})$$

where F_x is the effective force operator defined in Eq. (13) and $\bar{\mathcal{F}}_x$ denotes the equilibrium free energy of the quantum system, defined in Eq. (88).

This initial value problem can be solved by exploiting the fact that $\delta \bar{F}_x$ belongs to an invariant subspace of $\bar{\mathcal{L}}_x^\dagger$. To this end, we define a sequence of operators

$$\bar{\mathcal{L}}_x^\dagger \delta \bar{F}_x^1 = \delta \bar{F}_x^2, \quad \bar{\mathcal{L}}_x^\dagger \delta \bar{F}_x^2 = \delta \bar{F}_x^3, \quad \dots, \quad \bar{\mathcal{L}}_x^\dagger \delta \bar{F}_x^N = \delta \bar{F}_x^{N+1}. \quad (\text{A7})$$

If $\delta \bar{F}_x^{N+1}$ can be expressed as a linear combination of $\delta \bar{F}_x^1, \dots, \delta \bar{F}_x^N$, i.e., if there exists constants c_x^k so that $\delta \bar{F}_x^{N+1} = \sum_{k=1}^N c_x^k \delta \bar{F}_x^k$, the solution of Eq. (A5) can be written as

$$e^{\bar{\mathcal{L}}_x^\dagger \delta \bar{F}_x} = (1, 0, \dots, 0) \cdot e^{\mathbf{A}_x \delta \bar{\mathbf{F}}_x}, \quad (\text{A8})$$

where $\delta \bar{\mathbf{F}}_x = (\delta \bar{F}_x^1, \delta \bar{F}_x^2, \dots, \delta \bar{F}_x^N)^\text{T}$ and the matrix \mathbf{A}_x is given by

$$\bar{\mathcal{L}}_x^\dagger \delta \bar{\mathbf{F}}_x = \mathbf{A}_x \delta \bar{\mathbf{F}}_x. \quad (\text{A9})$$

Upon using the expressions (A3) and (A6), we find

$$\begin{aligned} \bar{\mathcal{L}}_x^\dagger \delta \bar{F}_x^1 &= -\frac{V'_x}{N} \sum_{k,l=1}^N \left\{ \bar{\chi}_x^+ \mathcal{K}^\dagger[\sigma_k^+] n_l n_{l+1} + \bar{\chi}_x^- \mathcal{K}^\dagger[\sigma_k^-] n_l n_{l+1} \right\} \\ &= -\frac{V'_x}{N} \left\{ -2\bar{\chi}^- \sum_{l=1}^N n_l n_{l+1} + \bar{\chi}^+ \sum_{l=1}^N (n_l g_{l+1} + g_l n_{l+1}) \right\} \\ &\equiv \delta \bar{F}_x^2, \end{aligned} \quad (\text{A10})$$

$$\begin{aligned} \bar{\mathcal{L}}_x^\dagger \delta \bar{F}_x^2 &= \frac{V'_x}{N} \sum_{k,l=1}^N \left\{ \left(\bar{\chi}_x^+ \mathcal{K}^\dagger[\sigma_k^+] + \bar{\chi}_x^- \mathcal{K}^\dagger[\sigma_k^-] \right) \left(2\bar{\chi}^- n_l n_{l+1} - \bar{\chi}^+ (n_l g_{l+1} + g_l n_{l+1}) \right) \right\} \\ &= -(3\bar{\chi}_x^- + \bar{\chi}_x^+) \delta \bar{F}_x^1 + \frac{2V'_x}{N} \left(\bar{\chi}_x^{-2} \sum_{l=1}^N n_l n_{l+1} - \bar{\chi}_x^{+2} \sum_{l=1}^N g_l g_{l+1} \right) \\ &\equiv \delta \bar{F}_x^3, \end{aligned} \quad (\text{A11})$$

$$\bar{\mathcal{L}}_x^\dagger \delta \bar{F}_x^3 = -3\bar{\chi} \delta \bar{F}_x^2 - 2\bar{\chi}_x^2 \delta \bar{F}_x^3, \quad (\text{A12})$$

with the coefficient matrix

$$\mathbf{A}_x = \begin{pmatrix} 0 & 1 & 0 \\ 0 & 0 & 1 \\ 0 & -3\bar{\chi}_x & -2\bar{\chi}_x^2 \end{pmatrix}. \quad (\text{A13})$$

This matrix can be easily exponentiated, which, upon insertion into the Eqs. (A8) and (A2) yields the compact expression

$$\bar{D}_x^{\text{qu}} = V_x'^2 \frac{\bar{\chi}_x^{+2} \bar{\chi}_x^- (8\bar{\chi}_x^+ + \bar{\chi}_x^-)}{2N \bar{\chi}_x^5}, \quad (\text{A14})$$

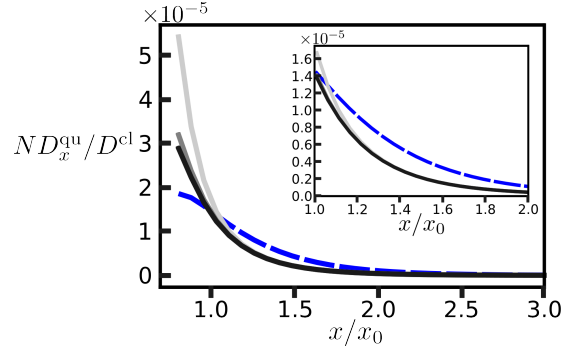


FIG. 5. Plot of MF and exact results for the quantum diffusion constant D_x^{qu} as a function of the normalized inter-atomic distance x/x_0 for the inverse temperature $\beta^{\text{qu}} = 0.1/\hbar\omega_a$. In the relevant regime, the behaviour of the MF result (blue dashed) is in good agreement with the exact plots, which are numerically determined for $N = 5$ (light grey), $N = 7$ (grey) and $N = 9$ (black). The inset highlights the results around the region where the typical trajectories of the two-stroke cycle occur in Figs. 3 and 4.

for the quantum diffusion constant in the mean-field approximation.

This result provides a useful benchmark for the quality of the mean-field approximation. For a quantitative comparison, we numerically solve the exact equation of motion, $\delta F_{x,t} = \mathbb{L}_x^\dagger \delta F_{x,t}$, for the shifted force operator in the Heisenberg picture and then evaluate D_x^{qu} with the help of Eq. (17). The results of this calculation are plotted in Fig. 5 for a relevant range of system parameters and Rydberg chains with $N = 5, 7, 9$ atoms. We find that, within the spatial region where the mirror settles during the two-stroke cycle described in Sec. IV, cf. Fig. 4, the mean-field and exact results are indeed in good agreement up to smaller deviations. In the limit $x \rightarrow 0$, the interaction potential V_x diverges and the mean-field approximation breaks down. However, within the situations discussed in the main text, x is effectively limited to a finite range around x_0 , where the interaction strength is still sufficiently weak for the mean-field approximation to be applicable.

2. Stochastic Dissipated Heat Current in the Mean-Field Picture

The three terms that appear in the expression (95c) for the stochastic dissipated heat current within the mean-field approximation are given by

$$\begin{aligned} \text{Tr}[H_x^{\text{qu}} \bar{\mathbb{L}}_x \bar{\rho}_x^{(x)}] &= \frac{1}{Nm} \text{Tr}[H_x^{\text{qu}} \bar{\varrho}_x^{\text{qu}'}] \\ &= \frac{1}{m} \frac{\bar{\chi}_x^-}{\bar{\chi}_x} \left\{ (\omega_a + 2 \frac{\bar{\chi}_x^+}{\bar{\chi}_x} V_x) (1 - \frac{\bar{\chi}_x^+}{\bar{\chi}_x}) \right\} \partial_x \left(\frac{\bar{\chi}_x^+}{\bar{\chi}_x^-} \right), \end{aligned} \quad (\text{A15a})$$

$$\begin{aligned} \text{Tr}[H_x^{\text{qu}} \bar{\mathbb{L}}_x \bar{\rho}_x^{(p)}] &= \frac{1}{N^2 m} \text{Tr}[H_x^{\text{qu}} \bar{\mathbb{L}}_x^{-1} \bar{\varrho}_x^{\text{qu}'}] \\ &= \int_0^\infty ds \text{Tr}[H_x^{\text{qu}} e^{\bar{\mathbb{L}}_x^\dagger s} \bar{\varrho}_x'] \\ &= - \frac{\bar{\chi}_x^{-2} (2V_x \bar{\chi}_x^+ + \omega_a \bar{\chi}_x)}{Nm \bar{\chi}_x^4} \partial_x \left(\frac{\bar{\chi}_x^+}{\bar{\chi}_x^-} \right), \end{aligned} \quad (\text{A15b})$$

$$\begin{aligned} \text{Tr}[H_x^{\text{qu}} \bar{\mathbb{L}}_x \bar{\rho}_x^{(2x)}] &= \frac{1}{Nm^2} \text{Tr}[H_x^{\text{qu}} (\bar{\mathbb{L}}_x^{-1} \bar{\varrho}_x^{\text{qu}'})'] \\ &= -\partial_x \left(\frac{\bar{\chi}_x^{-2} (2V_x' \bar{\chi}_x^+ + \omega_a \bar{\chi}_x)}{m^2 \bar{\chi}_x^4} \partial_x \left(\frac{\bar{\chi}_x^+}{\bar{\chi}_x^-} \right) \right) + 2V_x \frac{\bar{\chi}_x^{-2} \bar{\chi}_x^+}{m^2 \bar{\chi}_x^4} \partial_x \left(\frac{\bar{\chi}_x^+}{\bar{\chi}_x^-} \right). \end{aligned} \quad (\text{A15c})$$

Here, the first result follows immediately by inserting the expression (87) for the derivative of the mean-field steady state. The second result is obtained by first noting that $\bar{\mathbb{L}}_x \bar{\varrho}_x^{\text{qu}} \circ = \bar{\varrho}_x^{\text{qu}} \bar{\mathbb{L}}_x^\dagger \circ$ and then applying the same technique as for evaluation of the quantum-diffusion constant in the previous section. In the present case, only one auxiliary variable $\delta \bar{F}_x^{\hbar\omega_a, 2} = \bar{\mathbb{L}}_x^\dagger \bar{F}_x^{\hbar\omega_a}$ is necessary since $(\bar{\mathbb{L}}_x^\dagger)^2 \bar{F}_x^{\hbar\omega_a} = -\bar{\chi}_x \delta \bar{F}_x^{\hbar\omega_a}$, where $\delta \bar{F}_x^{\hbar\omega_a}$ was defined below Eq. (87). Finally,

Eq. (A15c) follows directly by applying the chain rule

$$\text{Tr}[H_x^{\text{qu}}(\bar{\mathbf{L}}_x^{-1}\bar{\varrho}_x^{\text{qu}})'] = \frac{d}{dx}\text{Tr}[H_x^{\text{qu}}\bar{\mathbf{L}}_x^{-1}\bar{\varrho}_x^{\text{qu}}] - \text{Tr}[H_x^{\text{qu}}\bar{\mathbf{L}}_x^{-1}\bar{\varrho}_x^{\text{qu}}] \quad (\text{A16})$$

and observing that

$$\text{Tr}[H_x^{\text{qu}}\bar{\mathbf{L}}_x^{-1}\bar{\varrho}_x^{\text{qu}}] = -2NV'_x \frac{\bar{\chi}_x^{-2}\bar{\chi}_x^+}{\bar{\chi}_x^4} \partial_x \left(\frac{\bar{\chi}_x^+}{\bar{\chi}_x^-} \right). \quad (\text{A17})$$

Appendix B: Numerical Simulations

To simulate the Langevin dynamics described by Eqs. (94), we implement a simple Euler-Maruyama method [128]. The iterative form of the Langevin equations in discretized time is

$$x_{n+1} = x_n + \Delta t \, p_n/m, \quad (\text{B1a})$$

$$p_{n+1} = p_n + \Delta t \left(-c(x_n - x_0) - \bar{\mathcal{F}}'_{x_n}/N^2 - (\beta^{\text{qu}}D_{x_n}^{\text{qu}} + \beta^{\text{cl}}D_{x_n}^{\text{cl}})p_n/m + \frac{1}{N} \left(\sqrt{\frac{2D_{x_n}^{\text{cl}}}{\Delta t}} G_{t_n}^{\text{cl}} + \sqrt{\frac{2D_{x_n}^{\text{qu}}}{\Delta t}} G_{t_n}^{\text{qu}} \right) \right), \quad (\text{B1b})$$

where $\Delta t = t_{n+1} - t_n$ denotes the time step and $G_t \sim \mathcal{N}(0, 1)$ is a random number sampled from a Gaussian distribution with mean 0 and variance 1. The superscript on the random variables $G^{\text{qu/cl}}$ indicates that the quantum or classical noise are statistically independent. Upon iterating these expressions over a specified time $\tau = N_{\text{steps}}\Delta t$, where N_{steps} is an integer, we can simulate the dynamics of the classical degree of freedom. At each time step, we recalculate the deterministic quantum force, the quantum diffusion constant and thus the magnitude of the Gaussian noise.

To calculate thermodynamic quantities, we use the Euler method of integration at the half time step, between the present and the previous iteration. This approach gives results that are correct up to corrections of order of Δt^3 . For a function that depends on some time dependent variable u_t , we have

$$\dot{f}_{u_t} \simeq \frac{f_{u_{n+1}} - f_{u_n}}{\Delta t} \equiv \frac{f_{u_n^+ + u_n^-} - f_{u_n^+ - u_n^-}}{\Delta t} \simeq 2\partial_u f_{u_n^+} \frac{u_n^-}{\Delta t} + \mathcal{O}(\Delta t^3), \quad (\text{B2})$$

where $u_n^+ = (u_{n+1} + u_n)/2$ and $u_n^- = (u_{n+1} - u_n)/2$. To calculate the time integrated work, exchange heat and dissipated heat and work associated with a single realization of a thermodynamic process, we use this rule to evaluate

$$w_{n+1} = w_n + 2V'_{x_n^+} \left(\frac{\bar{\chi}_{x_n^+}^+}{\bar{\chi}_{x_n^+}^-} \right)^2 x_n^-, \quad (\text{B3a})$$

$$q_{n+1}^{\text{ex}} = q_n^{\text{ex}} + 2\beta_n^{\text{qu}} (V'_{x_n^+})^2 \frac{\bar{\chi}_{x_n^+}^{+2}\bar{\chi}_{x_n^+}^- (8\bar{\chi}_{x_n^+}^+ + \bar{\chi}_{x_n^+}^-)}{2N\bar{\chi}_{x_n^+}^5} x_n^- p_n^+, \quad (\text{B3b})$$

$$q_{n+1}^{\text{d}} = q_n^{\text{d}} + 2\text{Tr}[H_{x_n^+}^{\text{qu}}\bar{\mathbf{L}}_{x_n^+}\bar{\rho}_{x_n^+}^{(x)}]x_n^- + 2\text{Tr}[H_{x_n^+}^{\text{qu}}\bar{\mathbf{L}}_{x_n^+}\bar{\rho}_{x_n^+}^{(2x)}]x_n^- p_n^+ + 2\text{Tr}[H_{x_n^+}^{\text{qu}}\bar{\mathbf{L}}_{x_n^+}\bar{\rho}_{x_n^+}^{(p)}]p_n^- + \varepsilon_{x_n^+, t_n}. \quad (\text{B3c})$$

Here, we have used that $f_{n+1} = f_n + \Delta t \dot{f}_t$ and replaced \dot{w}_t , \dot{q}_t^{ex} and \dot{q}_t^{d} with the expressions in Eq. (95). The full expressions in Eq. (B3c) can be found in (A15) and Eq. (55). All quantities are evaluated for fixed β^{qu} , except for at the switching time of the two stroke-cycle described in Sec. IV, where we set $\beta^{\text{qu}} = (\beta_h^{\text{qu}} + \beta_c^{\text{qu}})/2$ in the time step right after the temperature switch. Only in this particular situation, the term $\varepsilon_{x_n^+, t_n}$, which accounts for the relaxation of the quantum subsystem after an instantaneous temperature change, is non-zero, cf. Eq. (55).

-
- [1] R. Kosloff and A. Levy, Quantum heat engines and refrigerators: Continuous devices, *Annu. Rev. Phys. Chem.* **65**, 365 (2014).
 [2] S. Vinjanampathy and J. Anders, Quantum thermody-

- namics, *Contemp. Phys.* **57**, 545 (2016).
 [3] G. Benenti, G. Casati, K. Saito, and R. S. Whitney, Fundamental aspects of steady-state conversion of heat to work at the nanoscale, *Phys. Rep.* **694**, 1 (2017).

- [4] V. Mukherjee and U. Divakaran, Many-body quantum thermal machines, *J. Phys.: Condens. Matter* **33**, 454001 (2021).
- [5] N. M. Myers, O. Abah, and S. Deffner, Quantum thermodynamic devices: From theoretical proposals to experimental reality, *AVS Quantum Sci.* **4** (2022).
- [6] A. Ü. Hardal and Ö. E. Müstecaplıoğlu, Superradiant quantum heat engine, *Sci. Rep.* **5**, 12953 (2015).
- [7] R. Uzdin, Coherence-induced reversibility and collective operation of quantum heat machines via coherence recycling, *Phys. Rev. Appl.* **6**, 024004 (2016).
- [8] J. Jaramillo, M. Beau, and A. del Campo, Quantum supremacy of many-particle thermal machines, *New J. Phys.* **18**, 075019 (2016).
- [9] Y.-H. Ma, S.-H. Su, and C.-P. Sun, Quantum thermodynamic cycle with quantum phase transition, *Phys. Rev. E* **96**, 022143 (2017).
- [10] W. Niedenzu and G. Kurizki, Cooperative many-body enhancement of quantum thermal machine power, *New J. Phys.* **20**, 113038 (2018).
- [11] J. Li, T. Fogarty, S. Campbell, X. Chen, and T. Busch, An efficient nonlinear Feshbach engine, *New J. Phys.* **20**, 015005 (2018).
- [12] Y.-Y. Chen, G. Watanabe, Y.-C. Yu, X.-W. Guan, and A. del Campo, An interaction-driven many-particle quantum heat engine and its universal behavior, *npj Quantum Inf.* **5**, 88 (2019).
- [13] C. L. Latune, I. Sinayskiy, and F. Petruccione, Thermodynamics from indistinguishability: Mitigating and amplifying the effects of the bath, *Phys. Rev. Res.* **1**, 033192 (2019).
- [14] N. M. Myers and S. Deffner, Bosons outperform fermions: The thermodynamic advantage of symmetry, *Phys. Rev. E* **101**, 012110 (2020).
- [15] T. Keller, T. Fogarty, J. Li, and T. Busch, Feshbach engine in the Thomas-Fermi regime, *Phys. Rev. Res.* **2**, 033335 (2020).
- [16] G. Watanabe, B. P. Venkatesh, P. Talkner, M.-J. Hwang, and A. del Campo, Quantum statistical enhancement of the collective performance of multiple bosonic engines, *Phys. Rev. Lett.* **124**, 210603 (2020).
- [17] F. Carollo, F. M. Gambetta, K. Brandner, J. P. Garrahan, and I. Lesanovsky, Nonequilibrium quantum many-body Rydberg atom engine, *Phys. Rev. Lett.* **124**, 170602 (2020).
- [18] F. Carollo, K. Brandner, and I. Lesanovsky, Nonequilibrium many-body quantum engine driven by time-translation symmetry breaking, *Phys. Rev. Lett.* **125**, 240602 (2020).
- [19] T. Fogarty and T. Busch, A many-body heat engine at criticality, *Quantum Sci. Technol.* **6**, 015003 (2020).
- [20] N. M. Myers, J. McCready, and S. Deffner, Quantum heat engines with singular interactions, *Symmetry* **13** (2021).
- [21] M. Kloc, K. Meier, K. Hadjikyriakos, and G. Schaller, Superradiant many-qubit absorption refrigerator, *Phys. Rev. Appl.* **16**, 044061 (2021).
- [22] N. M. Myers, F. J. Peña, O. Negrete, P. Vargas, G. De Chiara, and S. Deffner, Boosting engine performance with Bose-Einstein condensation, *New J. Phys.* **24**, 025001 (2022).
- [23] J. Li, E. Y. Sherman, and A. Ruschhaupt, Quantum heat engine based on a spin-orbit- and Zeeman-coupled Bose-Einstein condensate, *Phys. Rev. A* **106**, L030201 (2022).
- [24] L. da Silva Souza, G. Manzano, R. Fazio, and F. Iemini, Collective effects on the performance and stability of quantum heat engines, *Phys. Rev. E* **106**, 014143 (2022).
- [25] P. J. Paulino, I. Lesanovsky, and F. Carollo, Nonequilibrium thermodynamics and power generation in open quantum optomechanical systems, *Phys. Rev. A* **108**, 023516 (2023).
- [26] M. A. Macovei, Performance of the collective three-level quantum thermal engine, *Phys. Rev. A* **105**, 043708 (2022).
- [27] D. Kolisnyk and G. Schaller, Performance boost of a collective qutrit refrigerator, *Phys. Rev. Appl.* **19**, 034023 (2023).
- [28] B. Yadin, B. Morris, and K. Brandner, Thermodynamics of permutation-invariant quantum many-body systems: A group-theoretical framework, *Phys. Rev. Res.* **5**, 033018 (2023).
- [29] U. Marzolino, Quantum thermochemical engines, *Phys. Rev. Appl.* **21**, 034003 (2024).
- [30] J. Eglinton, T. Pyhäranta, K. Saito, and K. Brandner, Thermodynamic geometry of ideal quantum gases: a general framework and a geometric picture of BEC-enhanced heat engines, *New J. Phys.* **25**, 043014 (2023).
- [31] A. d. Campo, J. Goold, and M. Paternostro, More bang for your buck: Super-adiabatic quantum engines, *Scientific reports* **4**, 6208 (2014).
- [32] P. Abiuso, H. J. D. Miller, M. Perarnau-Llobet, and M. Scandi, Geometric optimisation of quantum thermodynamic processes, *Entropy* **22** (2020).
- [33] H. J. D. Miller and M. Mehboudi, Geometry of work fluctuations versus efficiency in microscopic thermal machines, *Phys. Rev. Lett.* **125**, 260602 (2020).
- [34] B. Bhandari, P. T. Alonso, F. Taddei, F. von Oppen, R. Fazio, and L. Arrachea, Geometric properties of adiabatic quantum thermal machines, *Phys. Rev. B* **102**, 155407 (2020).
- [35] K. Brandner and K. Saito, Thermodynamic geometry of microscopic heat engines, *Phys. Rev. Lett.* **124**, 040602 (2020).
- [36] P. T. Alonso, P. Abiuso, M. Perarnau-Llobet, and L. Arrachea, Geometric optimization of nonequilibrium adiabatic thermal machines and implementation in a qubit system, *PRX Quantum* **3**, 010326 (2022).
- [37] J. Eglinton and K. Brandner, Geometric bounds on the power of adiabatic thermal machines, *Phys. Rev. E* **105**, L052102 (2022).
- [38] P. Menczel, T. Pyhäranta, C. Flindt, and K. Brandner, Two-stroke optimization scheme for mesoscopic refrigerators, *Phys. Rev. B* **99**, 224306 (2019).
- [39] A. Hartmann, V. Mukherjee, W. Niedenzu, and W. Lechner, Many-body quantum heat engines with shortcuts to adiabaticity, *Phys. Rev. Res.* **2**, 023145 (2020).
- [40] N. Pancotti, M. Scandi, M. T. Mitchison, and M. Perarnau-Llobet, Speed-ups to isothermality: Enhanced quantum thermal machines through control of the system-bath coupling, *Phys. Rev. X* **10**, 031015 (2020).
- [41] R. Xu, A numerical method to find the optimal thermodynamic cycle in microscopic heat engine, *J. Stat. Phys.* **184**, 29 (2021).

- [42] I. Khait, J. Carrasquilla, and D. Segal, Optimal control of quantum thermal machines using machine learning, *Phys. Rev. Res.* **4**, L012029 (2022).
- [43] P. A. Erdman and F. Noé, Identifying optimal cycles in quantum thermal machines with reinforcement-learning, *npj Quantum Inf.* **8**, 1 (2022).
- [44] A. Das, S. Mahunta, B. K. Agarwalla, and V. Mukherjee, Precision bound and optimal control in periodically modulated continuous quantum thermal machines, *Phys. Rev. E* **108**, 014137 (2023).
- [45] G.-x. Deng, H. Ai, B. Wang, W. Shao, Y. Liu, and Z. Cui, Exploring the optimal cycle for a quantum heat engine using reinforcement learning, *Phys. Rev. A* **109**, 022246 (2024).
- [46] P. Pietzonka and U. Seifert, Universal trade-off between power, efficiency, and constancy in steady-state heat engines, *Phys. Rev. Lett.* **120**, 190602 (2018).
- [47] M. Campisi, J. Pekola, and R. Fazio, Nonequilibrium fluctuations in quantum heat engines: theory, example, and possible solid state experiments, *New J. Phys.* **17**, 035012 (2015).
- [48] S. Saryal, M. Gerry, I. Khait, D. Segal, and B. K. Agarwalla, Universal bounds on fluctuations in continuous thermal machines, *Phys. Rev. Lett.* **127**, 190603 (2021).
- [49] J. Liu and D. Segal, Coherences and the thermodynamic uncertainty relation: Insights from quantum absorption refrigerators, *Phys. Rev. E* **103**, 032138 (2021).
- [50] H. J. D. Miller, M. H. Mohammady, M. Perarnau-Llobet, and G. Guarneri, Thermodynamic uncertainty relation in slowly driven quantum heat engines, *Phys. Rev. Lett.* **126**, 210603 (2021).
- [51] A. Rignon-Bret, G. Guarneri, J. Goold, and M. T. Mitchison, Thermodynamics of precision in quantum nanomachines, *Phys. Rev. E* **103**, 012133 (2021).
- [52] M. Gerry, N. Kalantar, and D. Segal, Bounds on fluctuations for ensembles of quantum thermal machines, *J. Phys. A* **55**, 104005 (2022).
- [53] Y. Xiao, D. Liu, J. He, L. Zhuang, W.-M. Liu, L.-L. Yan, and J. Wang, Thermodynamics and fluctuations in finite-time quantum heat engines under reservoir squeezing, *Phys. Rev. Res.* **5**, 043185 (2023).
- [54] A. Levy, L. Diósi, and R. Kosloff, Quantum flywheel, *Phys. Rev. A* **93**, 052119 (2016).
- [55] F. C. Binder, S. Vinjanampathy, K. Modi, and J. Goold, Quantacell: powerful charging of quantum batteries, *New J. Phys.* **17**, 075015 (2015).
- [56] A. Roulet, S. Nimmrichter, J. M. Arrazola, S. Seah, and V. Scarani, Autonomous rotor heat engine, *Phys. Rev. E* **95**, 062131 (2017).
- [57] S. Seah, S. Nimmrichter, and V. Scarani, Work production of quantum rotor engines, *New J. Phys.* **20**, 043045 (2018).
- [58] N. Van Horne, D. Yum, T. Dutta, P. Hänggi, J. Gong, D. Poletti, and M. Mukherjee, Single-atom energy-conversion device with a quantum load, *npj Quantum Inf.* **6**, 37 (2020).
- [59] W. S. Martins, F. Carollo, W. Li, K. Brandner, and I. Lesanovsky, Rydberg-ion flywheel for quantum work storage, *Phys. Rev. A* **108**, L050201 (2023).
- [60] H. Leitch, K. Hammam, and G. De Chiara, Thermodynamics of hybrid quantum rotor devices, *Phys. Rev. E* **109**, 024108 (2024).
- [61] D. von Lindenfels, O. Gräb, C. T. Schmiegelow, V. Kaushal, J. Schulz, M. T. Mitchison, J. Goold, F. Schmidt-Kaler, and U. G. Poschinger, Spin heat engine coupled to a harmonic-oscillator flywheel, *Phys. Rev. Lett.* **123**, 080602 (2019).
- [62] O. Abah, J. Roßnagel, G. Jacob, S. Deffner, F. Schmidt-Kaler, K. Singer, and E. Lutz, Single-ion heat engine at maximum power, *Phys. Rev. Lett.* **109**, 203006 (2012).
- [63] J. Roßnagel, S. T. Dawkins, K. N. Tolazzi, O. Abah, E. Lutz, F. Schmidt-Kaler, and K. Singer, A single-atom heat engine, *Science* **352**, 325 (2016).
- [64] Q. Bouton, J. Nettersheim, S. Burgardt, D. Adam, E. Lutz, and A. Widera, A quantum heat engine driven by atomic collisions, *Nat. Commun.* **12**, 2063 (2021).
- [65] J. Koch, K. Menon, E. Cuestas, S. Barbosa, E. Lutz, T. Fogarty, T. Busch, and A. Widera, A quantum engine in the BEC-BCS crossover, *Nature* **621**, 723 (2023).
- [66] M. Josefsson, A. Svilans, A. M. Burke, E. A. Hoffmann, S. Fahlvik, C. Thelander, M. Leijnse, and H. Linke, A quantum-dot heat engine operating close to the thermodynamic efficiency limits, *Nat. Nanotechnol.* **13**, 920 (2018).
- [67] A. Ronzani, B. Karimi, J. Senior, Y. Chang, J. Peltonen, C. Chen, and J. Pekola, Tunable photonic heat transport in a quantum heat valve, *Nat. Phys.* **14**, 991 (2018).
- [68] J. Kim, S.-h. Oh, D. Yang, J. Kim, M. Lee, and K. An, A photonic quantum engine driven by superradiance, *Nat. Photonics* **16**, 707 (2022).
- [69] J. P. Peterson, T. B. Batalhão, M. Herrera, A. M. Souza, R. S. Sarthour, I. S. Oliveira, and R. M. Serra, Experimental characterization of a spin quantum heat engine, *Phys. Rev. Lett.* **123**, 240601 (2019).
- [70] V. F. Lisboa, P. R. Dieguez, J. R. Guimarães, J. F. G. Santos, and R. M. Serra, Experimental investigation of a quantum heat engine powered by generalized measurements, *Phys. Rev. A* **106**, 022436 (2022).
- [71] P. Talkner, E. Lutz, and P. Hänggi, Fluctuation theorems: Work is not an observable, *Phys. Rev. E* **75**, 050102 (2007).
- [72] M. Esposito, U. Harbola, and S. Mukamel, Nonequilibrium fluctuations, fluctuation theorems, and counting statistics in quantum systems, *Rev. Mod. Phys.* **81**, 1665 (2009).
- [73] M. Campisi, P. Hänggi, and P. Talkner, Colloquium: Quantum fluctuation relations: Foundations and applications, *Rev. Mod. Phys.* **83**, 771 (2011).
- [74] P. Talkner and P. Hänggi, Aspects of quantum work, *Phys. Rev. E* **93**, 022131 (2016).
- [75] M. Perarnau-Llobet, E. Bäumer, K. V. Hovhannisyan, M. Huber, and A. Acin, No-go theorem for the characterization of work fluctuations in coherent quantum systems, *Phys. Rev. Lett.* **118**, 070601 (2017).
- [76] W. Niedenzu, M. Huber, and E. Boukobza, Concepts of work in autonomous quantum heat engines, *Quantum* **3**, 195 (2019).
- [77] S. L. Jacob, M. Esposito, J. M. Parrondo, and F. Barra, Quantum scattering as a work source, *Quantum* **6**, 750 (2022).
- [78] S. L. Jacob, G. T. Landi, M. Esposito, and F. Barra, Two-point measurement energy statistics from particle scattering, *Phys. Rev. Res.* **5**, 043160 (2023).
- [79] P. Strasberg and M. G. Díaz, Classical quantum stochastic processes, *Phys. Rev. A* **100**, 022120 (2019).
- [80] T. N. Sherry and E. C. G. Sudarshan, Interaction between classical and quantum systems: A new approach

- to quantum measurement. I, Phys. Rev. D **18**, 4580 (1978).
- [81] T. N. Sherry and E. C. G. Sudarshan, Interaction between classical and quantum systems: A new approach to quantum measurement. II. Theoretical considerations, Phys. Rev. D **20**, 857 (1979).
- [82] W. Boucher and J. Traschen, Semiclassical physics and quantum fluctuations, Phys. Rev. D **37**, 3522 (1988).
- [83] C.-I. Kuo and L. H. Ford, Semiclassical gravity theory and quantum fluctuations, Phys. Rev. D **47**, 4510 (1993).
- [84] A. Anderson, Quantum backreaction on "classical" variables, Phys. Rev. Lett. **74**, 621 (1995).
- [85] O. V. Prezhdo and V. V. Kisil, Mixing quantum and classical mechanics, Phys. Rev. A **56**, 162 (1997).
- [86] L. Diósi and J. J. Halliwell, Coupling classical and quantum variables using continuous quantum measurement theory, Phys. Rev. Lett. **81**, 2846 (1998).
- [87] J. Caro and L. L. Salcedo, Impediments to mixing classical and quantum dynamics, Phys. Rev. A **60**, 842 (1999).
- [88] L. Diósi, N. Gisin, and W. T. Strunz, Quantum approach to coupling classical and quantum dynamics, Phys. Rev. A **61**, 022108 (2000).
- [89] R. Kapral, Progress in the theory of mixed quantum-classical dynamics, Annu. Rev. Phys. Chem. **57**, 129 (2006).
- [90] C. Barceló, R. Carballo-Rubio, L. J. Garay, and R. Gómez-Escalante, Hybrid classical-quantum formulations ask for hybrid notions, Phys. Rev. A **86**, 042120 (2012).
- [91] L. L. Salcedo, Statistical consistency of quantum-classical hybrids, Phys. Rev. A **85**, 022127 (2012).
- [92] L. Diósi, Hybrid quantum-classical master equations, Phys. Scr. **2014**, 014004 (2014).
- [93] R. Kapral, Quantum dynamics in open quantum-classical systems, J. Phys.: Condens. Matter **27**, 073201 (2015).
- [94] I. Burghardt, R. Carles, C. F. Kammerer, B. Lasorne, and C. Lasser, Separation of scales: dynamical approximations for composite quantum systems, J. Phys. A **54**, 414002 (2021).
- [95] J. Oppenheim, C. Sparaciari, B. Šoda, and Z. Weller-Davies, The two classes of hybrid classical-quantum dynamics, arXiv:2203.01332 (2022).
- [96] J. Oppenheim and Z. Weller-Davies, Path integrals for classical-quantum dynamics, arXiv:2301.04677 (2023).
- [97] I. Layton, J. Oppenheim, and Z. Weller-Davies, A healthier semi-classical dynamics, arXiv:2208.11722 (2022).
- [98] L. Diósi, Hybrid completely positive Markovian quantum-classical dynamics, Phys. Rev. A **107**, 062206 (2023).
- [99] A. D. B. Manjarres, M. Reginatto, and S. Ulbricht, Three statistical descriptions of classical systems and their extensions to hybrid quantum-classical systems, arXiv:2403.07738 (2024).
- [100] L. D'Alessio and A. Polkovnikov, Emergent Newtonian dynamics and the geometric origin of mass, Ann. Phys. **345**, 141 (2014).
- [101] Q. Zhang and B. Wu, General approach to quantum-classical hybrid systems and geometric forces, Phys. Rev. Lett. **97**, 190401 (2006).
- [102] M. Thomas, T. Karzig, S. V. Kusminskiy, G. Zaránd, and F. von Oppen, Scattering theory of adiabatic reaction forces due to out-of-equilibrium quantum environments, Phys. Rev. B **86**, 195419 (2012).
- [103] V. Cavina, A. Mari, and V. Giovannetti, Slow dynamics and thermodynamics of open quantum systems, Phys. Rev. Lett. **119**, 050601 (2017).
- [104] H. J. D. Miller, M. Scandi, J. Anders, and M. Perarnau-Llobet, Work fluctuations in slow processes: Quantum signatures and optimal control, Phys. Rev. Lett. **123**, 230603 (2019).
- [105] U. Seifert, Stochastic thermodynamics: principles and perspectives, Eur. Phys. J. B **64**, 423 (2008).
- [106] U. Seifert, Stochastic thermodynamics, fluctuation theorems and molecular machines, Rep. Prog. Phys. **75**, 126001 (2012).
- [107] U. Seifert, Stochastic thermodynamics: From principles to the cost of precision, Physica **504**, 176 (2018).
- [108] M. Aspelmeyer, T. J. Kippenberg, and F. Marquardt, Cavity optomechanics, Rev. Mod. Phys. **86**, 1391 (2014).
- [109] K. W. Murch, K. L. Moore, S. Gupta, and D. M. Stamper-Kurn, Observation of quantum-measurement backaction with an ultracold atomic gas, Nat. Phys. **4**, 561 (2008).
- [110] F. Brennecke, S. Ritter, T. Donner, and T. Esslinger, Cavity optomechanics with a Bose-Einstein condensate, Science **322**, 235 (2008).
- [111] M. H. Schleier-Smith, I. D. Leroux, H. Zhang, M. A. Van Camp, and V. Vuletić, Optomechanical cavity cooling of an atomic ensemble, Phys. Rev. Lett. **107**, 143005 (2011).
- [112] E. Gavartin, R. Braive, I. Sagnes, O. Arcizet, A. Beveratos, T. J. Kippenberg, and I. Robert-Philip, Optomechanical coupling in a two-dimensional photonic crystal defect cavity, Phys. Rev. Lett. **106**, 203902 (2011).
- [113] A. Youssefi, S. Kono, A. Bancora, M. Chegnizadeh, J. Pan, T. Vovk, and T. J. Kippenberg, Topological lattices realized in superconducting circuit optomechanics, Nature **612**, 666 (2022).
- [114] C. S. Adams, J. D. Pritchard, and J. P. Shaffer, Rydberg atom quantum technologies, J. Phys. B **53**, 012002 (2019).
- [115] R. Kubo, M. Toda, and N. Hashitsume, *Statistical physics II: nonequilibrium statistical mechanics*, Vol. 31 (Springer Science & Business Media, 2012).
- [116] Since $\varrho_x^{\text{qu}'}$ and $\rho_x^{(x)'}$ have vanishing trace and therefore are orthogonal to ϱ_x^{qu} , with respect to the scalar product, $\langle X|Y \rangle = \int_0^1 d\lambda \text{Tr}[\varrho_x^{\text{qu}1-\lambda} X^\dagger \varrho_x^{\text{qu}\lambda} Y]$, which renders the super operator \mathcal{L}_x self adjoint.
- [117] J. L. Alonso, C. Bouthelie, A. Castro, J. Clemente-Gallardo, and J. A. Jover-Galtier, Entropy and canonical ensemble of hybrid quantum classical systems, Phys. Rev. E **102**, 042118 (2020).
- [118] E. H. Lieb, Convex trace functions and the Wigner-Yanase-Dyson conjecture, Adv. in Math. **11**, 267 (1973).
- [119] H. Spohn, Entropy production for quantum dynamical semigroups, J. Math. Phys. **19**, 1227 (1978).
- [120] M. Marcuzzi, M. Buchhold, S. Diehl, and I. Lesanovsky, Absorbing state phase transition with competing quantum and classical fluctuations, Phys. Rev. Lett. **116**, 245701 (2016).
- [121] C. Nill, K. Brandner, B. Olmos, F. Carollo, and I. Lesanovsky, Many-body radiative decay in strongly

- interacting Rydberg ensembles, *Phys. Rev. Lett.* **129**, 243202 (2022).
- [122] M. Hoening, W. Abdussalam, M. Fleischhauer, and T. Pohl, Antiferromagnetic long-range order in dissipative Rydberg lattices, *Phys. Rev. A* **90**, 021603 (2014).
 - [123] V. Holubec, An exactly solvable model of a stochastic heat engine: optimization of power, power fluctuations and efficiency, *J. Stat. Mech.* **2014**, P05022 (2014).
 - [124] M. Müller, L. Liang, I. Lesanovsky, and P. Zoller, Trapped Rydberg ions: from spin chains to fast quantum gates, *New J. Phys.* **10**, 093009 (2008).
 - [125] G. Higgins, W. Li, F. Pokorny, C. Zhang, F. Kress, C. Maier, J. Haag, Q. Bodart, I. Lesanovsky, and M. Hennrich, Single Strontium Rydberg ion confined in a paul trap, *Phys. Rev. X* **7**, 021038 (2017).
 - [126] G. Higgins, F. Pokorny, C. Zhang, Q. Bodart, and M. Hennrich, Coherent control of a single trapped Rydberg ion, *Phys. Rev. Lett.* **119**, 220501 (2017).
 - [127] R. Kapral, Surface hopping from the perspective of quantum-classical Liouville dynamics, *Chem. Phys.* **481**, 77 (2016).
 - [128] C. W. Gardiner *et al.*, *Handbook of stochastic methods*, Vol. 3 (springer Berlin, 1985).